Engineering and Technology Journal
Journal homepage: https://etj.uotechnology.edu.iq

Reducing the surface roughness of curvature surfaces by electrical discharge machining with magnetic abrasive finishing

Shahd A. Taqi[a*], **Saad K. Shather**[a], **Wisam K. Hamdan**[b]

[a] College of Production Engineering and Metallurgy, University of Technology-Iraq, Alsina'a street, 10066 Baghdad, Iraq.
[b] College of Biomedicine, University of Technology-Iraq, Alsina'a street, 10066 Baghdad, Iraq.
*Corresponding author Email: pme.20.87@grad.uotechnology.edu.iq

HIGHLIGHTS

- Complex 3D models were designed in SolidWorks and fabricated using CNC machining.
- EDM was applied to study the effects of current, pulse on-time, and gap on MRR and roughness.
- Current was found to be the most dominant factor affecting MRR and surface roughness.
- GRA optimization identified the best condition for balancing the removal rate and surface finish.
- Magnetic abrasive finishing improved surface roughness by up to 64.02% with hybrid abrasives.

Keywords:
Electrical discharge machining
Magnetic abrasive finishing
Complex shapes
Hybrid particles
Improved surface roughness

ABSTRACT

This study presents an integrated work that combines unconventional machining and finishing techniques for complex geometric models. A Taguchi design investigated three electrical-discharge parameters—electric current, pulse duration, and gap—each at three levels; a multi-objective optimization matrix was then used to select the optimal conditions. The geometric models were designed using SolidWorks software and machined on a CNC machine to ensure maximum accuracy in the resulting samples. The samples were finished using the magnetic abrasive finishing technique, where the particle mixture was developed as a hybrid blend of two types of abrasive particles, tungsten carbide (WC) and silicon carbide (SiC). Among the electrical discharge machining factors, electric current showed the highest influence, yielding a maximum metal removal rate of 25.1024 mm³/min at Ip = 42 A, Tn = 300 µs, gap = 8 mm, and the minimum roughness of 11.6674 µm at Ip = 24 A, Tn = 150 µs, gap = 5 mm. The magnetic abrasive finishing stage substantially improved the surface quality of the complex models, reducing roughness from 11.9169 µm to about 4.29 µm, equivalent to a 64.02% reduction. Within finishing, feed rate was the most influential variable, followed by spindle speed, while particle size had the least effect. Overall, the combined methodology improves process performance and post-process surface quality for complex geometries while identifying the dominant parameters that govern material removal and roughness outcomes.

1. Introduction

The increasing development of modern industries has created a demand for complex geometric models with high precision and smooth surfaces. Since one of the essential requirements of advanced industries is the accuracy of complex surfaces, unconventional design and manufacturing techniques have become necessary to keep pace with these developments [1]. However, finishing complex surfaces and edges remains a challenge, as conventional approaches cannot adequately process all features. In addition, most available inspection methods are limited to flat surfaces or require cutting complex samples into smaller parts, which results in mechanical damage [2]. Although traditional manufacturing methods are efficient, they encounter limitations when dealing with hard or brittle materials and intricate geometries [3]. Therefore, this research holds importance from both scientific and applied perspectives, as it represents a significant step toward enhancing complex surfaces through unconventional machining and finishing processes.

Among modern design tools, SolidWorks has emerged as one of the most effective platforms for creating complex 3D models with high accuracy, enabling virtual design, testing, and modification before manufacturing [4,5]. The working principle of electrical discharge machining involves removing metal through repeated electric sparks generated between two electrodes (the cutting tool and the workpiece), separated by a work gap and immersed in an insulating medium, such as a dielectric fluid [6]. Each spark produces a significant temperature increase. Consequently, this heat causes the surface molecules of the sample to melt and vaporize. With repeated sparks, the temperature rises further, helping to remove the surface layer of the workpiece. In this regard, these high temperatures not only remove surface molecules but also affect the underlying area, which can cause

http://doi.org/10.30684/etj.2025.162757.1985
Received 25 July 2025; Received in revised form 04 September 2025; Accepted 09 September 2025; Available online 19 November 2025
2412-0758/University of Technology-Iraq, Baghdad, Iraq

subsurface deformation [7]. These effects often lead to irregular textures and thermal damage, which reduce performance and fatigue life [8]. To overcome these drawbacks, magnetic abrasive finishing (MAF) has been employed as an unconventional finishing process that uses magnetic force to align abrasive particles into a flexible brush, thereby removing burrs and enhancing the surface [9,10]. In particular, this process is highly effective for finishing internal cavities, complex geometric designs, and precision parts used in the medical and optical industries. Due to the flexibility of the finishing brush, it can finish most geometric complexities and curves [11]. The presence of abrasive particles plays a significant role in this regard, since the type, hardness, and size of the abrasive particles (e.g., SiC and Al_2O_3) have a direct impact on surface integrity, material removal efficiency, and resulting surface quality. Conventional inspection techniques are inadequate for use with such complex geometries, particularly in curved surfaces or hollow regions that are inaccessible to contact-type tools. For this reason, measurements of surface roughness with high accuracy are increasingly performed by non-contact methods [12], such as three-dimensional laser scanning. This technique relies on the principle of shining a laser beam onto the surface of the sample to be inspected. The laser is then reflected off the sample surface, and the laser beam is analyzed and received by a special camera. This camera converts these beams into data and surface topography maps, which are transmitted to a computer. Next, image processing applications are used to process this data to help compile it and provide the corresponding surface roughness values [13].

Several studies have investigated this topic, but most have not examined complex shapes. As an illustration, Kumar et al. [14], studied the effects of electrical discharge machining on various shapes and designs and its impact on material removal rate, tool wear rate, and surface quality. It was concluded that the circular electrode achieves superior surface finish quality, in addition to minimal tool wear. In addition, Huang and Sheu [15], studied the relationship between the cross-sectional shape of materials and their metal removal ability during machining processes. The research presented different cross-sectional shapes for several cutting tools. It was demonstrated that process performance varies depending on the cutting tool shape, with tool wear increasing as pulse time and current strength increase. At the same time, both factors contribute to the removal of larger particles. Study conducted by Laibi and Shather [16], analyzed the effect of electrode material type and process variables on the performance of the electrical discharge process; the material removal rate increased with higher current and shorter pulse durations, achieving 0.0367 g/min at 8 A and 25 µs. The optimum conditions of SR 1.38 µm were 1.5 A and 12 µs [17], highlighted the development of tools used in the EDM process through advanced methods to achieve high efficiency and accuracy and to obtain tools for complex shapes; it explored reducing the cost and time, and utilizing additional technologies to produce items challenging to manufacture using traditional methods. Uddin et al. [18], the impact of various factors of MAF was investigated using SiC and Al_2O_3 as the abrasive particles. Surface quality enhancements and influencing variables demonstrated varying levels of progress depending on the selection of the abrasive material during the study. The amount of abrasive used in conjunction with the rotation speed had the most substantial impact when using SiC, and when using Al_2O_3, the working space, along with the mesh size, had the most significant effect on its performance. Ahmad et al. [19], examined the development of the MAF process by creating magnetic abrasive compounds from two different types to benefit from their distinct features for modifying the abrasive component. The experimental mixture contained (Al_2O_3) at 25% together with (SiO_2) at 15% along with carbonyl iron powder at 60%. Experiments showed roughness decreased from 1.14 µm to 0.85 µm; surface quality improves when the manufactured magnetic abrasive (SMA) is implemented. In addition, Zou et al. [20], highlighted the development of MAF processes capable of improving the complex shapes of difficult-to-process materials and explored operational variables. They studied the combination of magnetic abrasive finishing (MAF) and fixed abrasive finishing (FAP) (MAF-FAP), achieving a significant improvement in roughness from 11.202 nm to 3.67 nm within 30 minutes. In another work Kumar and Komma [21], presented the development of the MAF process by installing finishing tools on the CNC machine to improve the surface quality of complex shapes; studied rotation speed (400, 600, 800)rpm, number of abrasive mesh size (400, 600, 1200), and working gap (2, 3, 4) mm. The number of abrasive meshes had the most significant effect (42.32%), followed by the gap (37.37%) and the rotation speed (2.07%); optimum parameters were 800 rpm, 600 mesh, and a clearance of 2 mm. Furthermore Shao et al. [22], focused on evaluation methods for surface texture and roughness inspection by introducing a novel approach analyzing laser beam reflection patterns through observation of scattering patterns produced by reflected beams; explored optical techniques as non-traditional, non-destructive, contact-free roughness measurement strategies, with the roughness pattern method being a precise measurement method; focused on the spot contrast approach with user-friendly operation and accurate results; recorded surface patterns by CCD cameras; measured roughness by analyzing light intensity and scattering similarity to diffraction, as the light intensity distribution indicates how the distribution of surface bumps influences roughness evaluation; the technique measured surface structure symmetry and consistency for precise quality evaluation of manufactured products and functioned through a non-contact methodology at high speed.

This study focuses on integrating two non-conventional processes, machining and finishing techniques, to determine how complementary these processes are and whether the surface roughness of the models improves when applying hybrid magnetic abrasive finishing. Because the study is non-conventional and the models are not simple, and since they cannot be inspected with conventional roughness testers, non-contact laser scanning was adopted to evaluate surface roughness after machining and after finishing.

2. Methodology

The specimen models were developed in three dimensions using SolidWorks, with consideration given to the complexity of the geometric shape to ensure an accurate representation of the industrial conditions. Particularly, the Electrical Discharge Machining (EDM) was used to produce specimens, which were then subjected to EDM with different machining parameters in an academically considered experimental procedure. The preliminary surface checks were then conducted using laser scanning, and the results were interpreted to evaluate the impact of the machining parameters on surface roughness. Subsequently, a finishing process, magnetic abrasive particle finishing (MAF), was employed after machining to achieve a superior finish. Then, the samples were once again laser-scanned, and the final data were differentiated to evaluate the efficiency of the finishing process compared to the first one after machining.

3. Experimental work

3.1 Design and implementation of shape

This phase involves designing working models for machining and finishing experiments, as well as creating the cutting tools required for the electrical discharge machining process and the magnetic finishing tools used for the finishing experiments. In this regard, the design phase of the working sample and the tool is critical, as it determines the degree of geometric complexity. The SolidWorks application was used to implement the design phase. A method such as drilling and cutting was used to perform EDM operations, facilitating assembly and reducing time, as the tool design closely resembled the working sample. In particular, the sample design was irregular, featuring curves, peaks, and troughs, which represented models closely related to industrial applications that are challenging to handle with traditional methods. A workpiece with 20 mm length × 15 mm width was used; the highest peak is 5 mm, and the lowest trough is 2 mm. The EDM tool width was 13 mm; it was intentionally undersized relative to the nominal feature span to minimize workpiece edge distortions induced by tool edges. To this end, the finishing tool is the primary component. It is responsible for generating the magnetic field that attracts the abrasive particles, forming what is known as the abrasive brush that performs the finishing process. During the design phase, grooves were drilled in the shaft to match the dimensions of the magnets used. A cover was designed for these magnetic locations to prevent them from moving during the finishing process. Figure 1 SolidWorks design models related to EDM, a) The design of the EDM cutting tool, b) The design of the EDM workpiece. Figure 2 SolidWorks design process of the MAF finishing tool, a) The tool with designed grooves, b) The tool with magnetic pieces added, c) The assembled configuration of the finishing tool, and d) The final completed tool geometry.

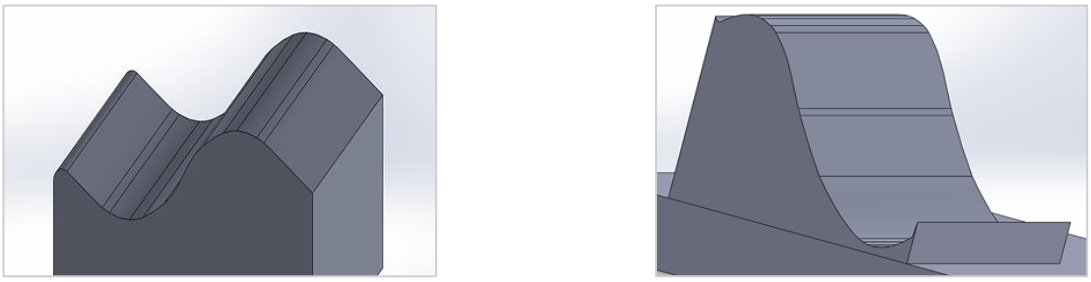

Figure 1: SolidWorks design models related to EDM: a) the EDM cutting tool; b) the EDM workpiece

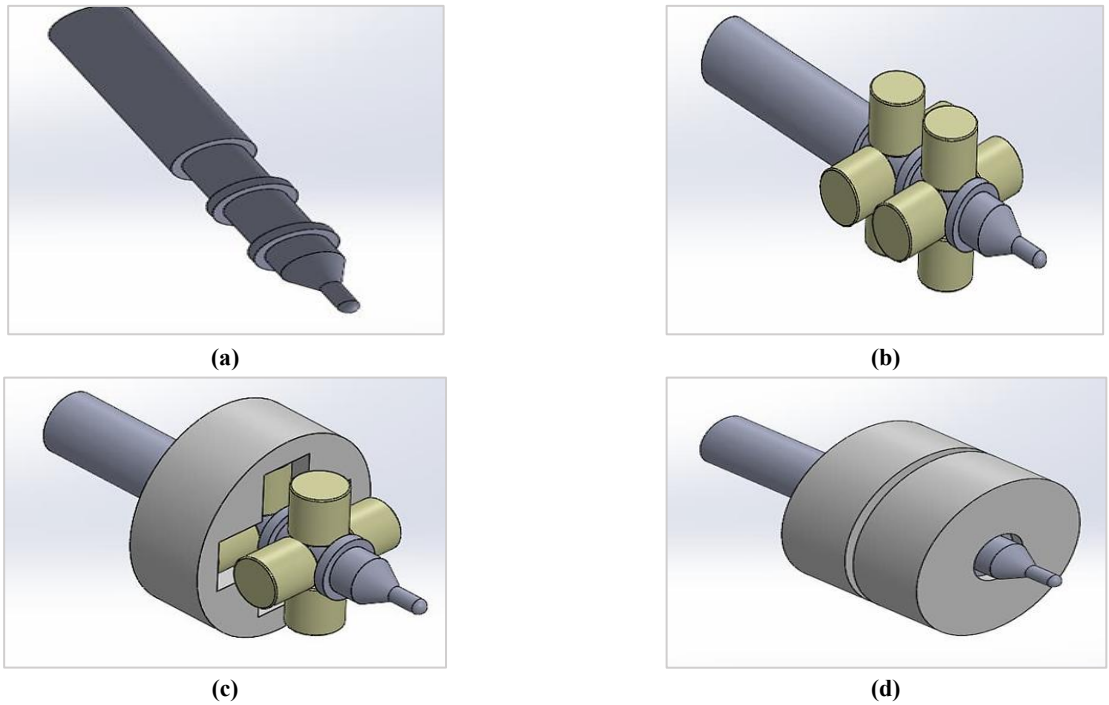

Figure 2: SolidWorks design process of the MAF finishing tool: a) tool with designed grooves b) tool with magnetic pieces added c) assembled configuration of the finishing tool, and d) final completed tool geometry

To implement models with a CNC machine, it is necessary to convert these designs into a language that the machine can understand. Therefore, these designs are converted into code using the HSMWorks program, which serves as a link between design and implementation. This code, known as G-code, determines the tool path and speed during execution. The model was then physically implemented using a three-axis CNC machine in the University of Technology's Lathe Workshop. This machine can move in three axes (X, Y, and Z), making it ideal for manufacturing complex shapes containing cavities and curves. More precisely, the models were made using a three-axis vertical CNC milling machine.

3.2 The EDM machining stage

At this stage, the components required for the EDM process are prepared and identified. The diagram in Figure 3 illustrates the workflow of the EDM process, starting from the selection of tool materials and workpiece samples, and the identification of process variables and their corresponding levels. After the Taguchi calculation, the experimental design is made, and then the machining operation is carried out by an EDM machine. The evaluation stage then involves assessing surface roughness (SR), material removal rate (MRR), and potential surface imperfections. Finally, the value of the optimization level is obtained from the Grey Relational Analysis (GRA).

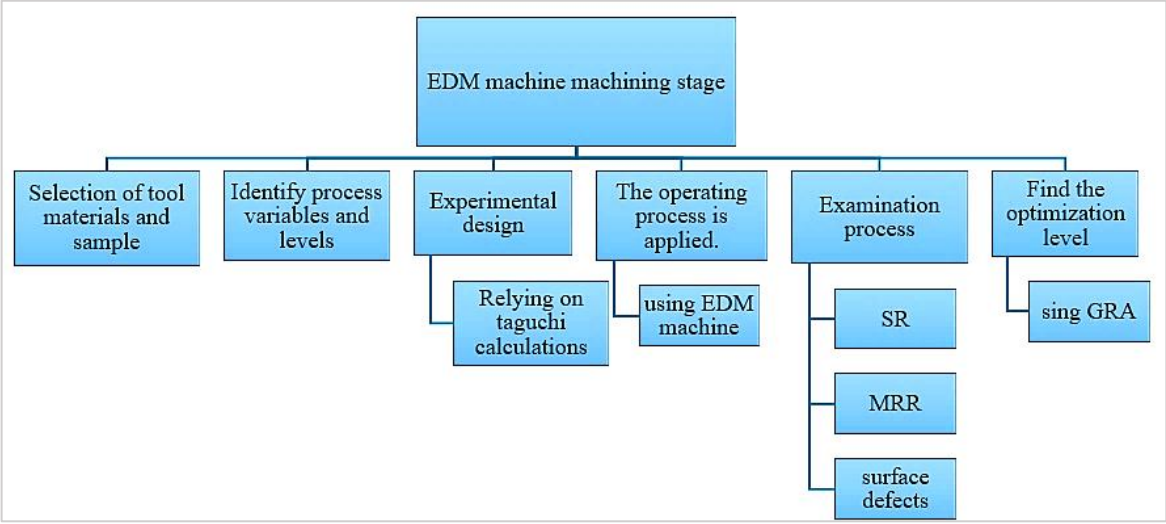

Figure 3: Diagram of the EDM stage

When selecting the material for the workpiece and tools to be used at this stage, several considerations must be made to ensure a successful machining process. Specifically, the electrical conductivity is of utmost importance in the selected material, ensuring spark generation and the ability to withstand high temperatures. In this regard, it is necessary to choose the electrical conductivity carefully because it affects the performance of the process [23]. Accordingly, the high-carbon steel was chosen as the primary material for the workpiece, while copper was used as the machining tool. Figure 4 Workpiece and EDM cutting tools used in the experimental work a) The prepared workpiece after machining, showing the geometry produced for the experiments, b) Copper EDM cutting tool, side view, and c) Copper EDM cutting tool, front view, highlighting the machined profile.

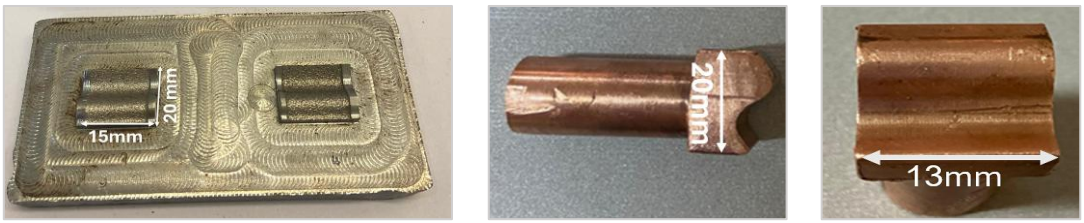

(a) **(b)** **(c)**

Figure 4: Tools and workpieces used in the practical experiments: a) prepared workpiece after machining, showing the produced geometry, b) copper EDM cutting tool, side view, c) copper EDM cutting tool, front view (13 mm) highlighting the machined profile

The phase of determining the operational variables identified during the experiments is a crucial step, as it facilitates the analysis of the effect of these variables on the process response. Particularly, three variables were identified at three levels. The pulse duration represents the amount of time the spark is glowing and shining on the surface, and is a crucial factor in the discharge process [24]. As for the current, it represents the amount of spark energy, and thus, it is necessary to take care of it when determining the levels of variables [25]. The Taguchi methodology was used to design experiments, as it helps reduce the number of experiments required while maintaining analytical capability. Table 1 shows the Takauji design table for operational experiments, which includes the variables and their levels.

After completing the previous steps and determining all process variables, the EDM test phase begins. All samples are machined at this stage using a CHMER EDM machine, model CM323C, and a CNC EDM controller. The inspection process represents a pivotal stage following the completion of the machining process. This stage assesses the quality of the process and identifies all potential factors that may impact its performance and efficiency. In particular, the inspection focused on three main outcomes:

1) Material Removal Rate: This outcome refers to the amount of material removed from the workpiece during machining. It is considered one of the most important productivity indicators for machining processes, reflecting the processing

ability to achieve an optimal balance between speed and accuracy. Specifically, it is calculated by subtracting the sample weight before and after machining from the machining time.

2) Surface Roughness: This roughness is the most important indicator for assessing the quality of a machining surface. It describes the microscopic protrusions or ripples that appear on the surface because of machining. It is a crucial outcome for evaluating the precision and smoothness of the product. In this study, laser scanning and reflected wavelengths were employed as an alternative to traditional roughness testing methods. Figure 5 Schematic drawing of the laser scanning material surface roughness measurement system. The system includes a light source projected at the roughness surface; the reflected signals are detected by the image acquisition unit in the machine vision system. The data obtained are processed in the computer system to produce speckle patterns. Then, from the data, feature extraction is performed in the data processing system to determine surface characteristics.

3) Surface Defects: This step supports the assessment of the surface structure of samples, defects, and gaps resulting from machining. The most common test for this outcome is the scanning electron microscope (SEM), one of the most advanced tools in microscopic analysis.

Table 1: The design of the experiments

No.	Current (A)	Ton (µs)	Gap (µm)
1	24	150	5
2	24	200	8
3	24	300	10
4	36	150	8
5	36	200	10
6	36	300	5
7	42	150	10
8	42	200	5
9	42	300	8

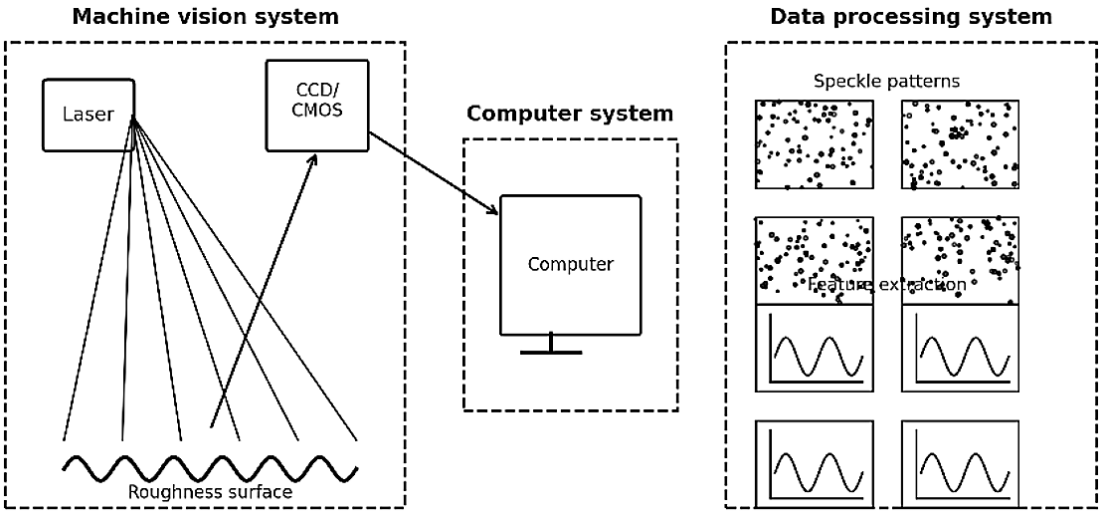

Figure 5: Schematic of the non-contact laser scanning setup used in this work (created by the authors)

After examining and obtaining the results of the data analysis phase, the data is extracted from the experiments. This step involves recording and discussing the results, as well as statistically analyzing them to determine the level of influence of each variable and the most important factor in the process. During this study, Minitab 18 was used to perform statistical analysis based on the Taguchi Method, an effective method in Design of Experiments (DOE) that helps improve quality and increase efficiency with the fewest possible experiments. However, the statistical analysis in this process does not determine which experiment contains the optimal conditions, as both the highest metal removal rate and the lowest surface roughness criteria are optimal. Therefore, multi-objective optimization is applied. Due to the multiple outputs and the different desired trends (the lowest roughness and the highest metal removal rate), a multi-objective optimization method was chosen and adopted to achieve the most effective balance between the operating variables. More precisely, a grayscale relationship analysis was used to evaluate the relationship between the variables. After determining the optimal variable level that yields a product with the best roughness and the highest metal removal rate, the variables are stabilized, and additional samples are manufactured. These are then reprocessed and run again in the EDM machine, all with the same variables. This process is performed to prepare for the next step, which is the finishing process. This step is undertaken to obtain accurate readings, rather than random ones, as the magnetic finishing process uses variable ball bearings.

3.3 The MAF Stage

This study is based on a systematic series that begins with the manufacture of samples with complex shapes, followed by the use of the electrical discharge spark cutting (EDM) technology. Finally, these samples are finished using the magnetic abrasive particle finishing technology to determine the effect of finishing on the manufactured samples. However, the available finishing processes lack the flexibility to handle complex shapes efficiently. This stage marks the beginning of the finishing process, and Figure 6 is a diagram of the MAF (Magnetic Abrasive Finishing) step. The production process starts with the production of the finishing tool (shaft preparation and use of a fixed magnet) and the preparation of abrasive particles. The subsequent step is to identify operating variables and design experiments using the Taguchi method. The CNC machine is then used for polishing. Finally, the results of the process are analyzed in the examination stage to check the material removal rate (MRR), surface roughness (SR), and possible surface defects.

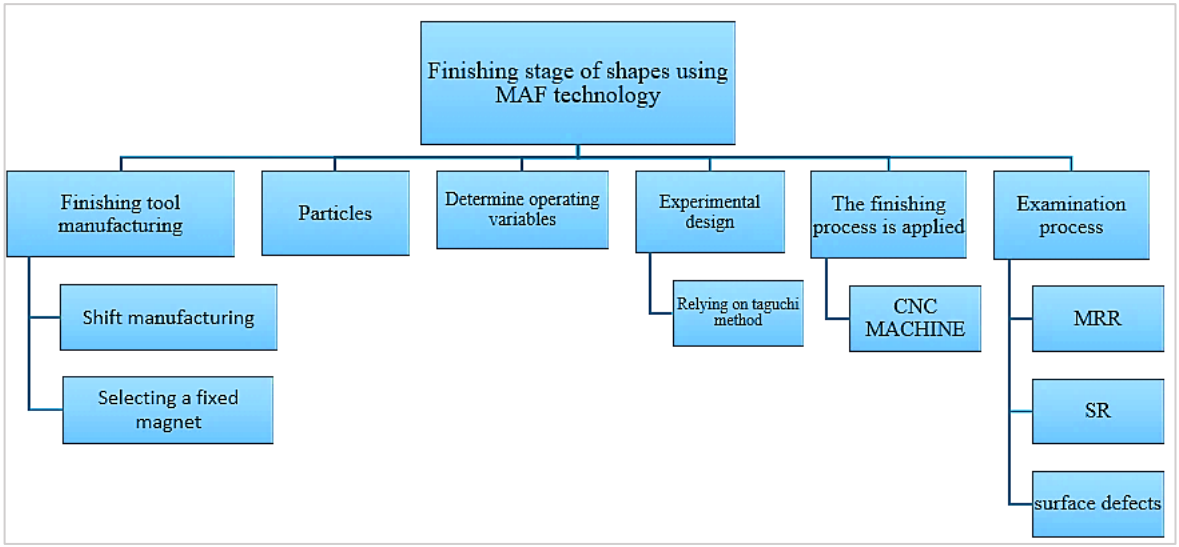

Figure 6: Diagram of the MAF stage

In this work, the shaft material was selected to match the workpiece, ensuring mechanical and thermal compatibility. This selection helps stabilize the tool during the finishing process. In particular, a type of magnet known as a neodymium magnet was chosen, as it is one of the strongest permanent magnets available, due to its high efficiency in generating a very high magnetic field relative to its small size. They were installed in the holes drilled in the shaft in a direction that allowed the abrasive particles to be attracted with the maximum force generated. Recently, a permanent external magnet has been utilized as a tool to generate a magnetic force because it is easily obtainable with the required strength, is easier to use, lighter in weight, and provides ease of adjusting the voltage distribution and cohesion of the particles [26]. The magnets were distributed symmetrically within the shaft, preventing rotational balance and avoiding deflection or vibration during finishing. Figure 7 shows the ultimate shape of the magnetic abrasive finishing (MAF) tool. The tool assembly comprises the shaft, the fixed magnet, and mounted magnetic pieces adapted to hold the abrasive particles during the finishing process. This setup is stable and can effectively transmit magnetic force to carry out surface finishing on complex geometries.

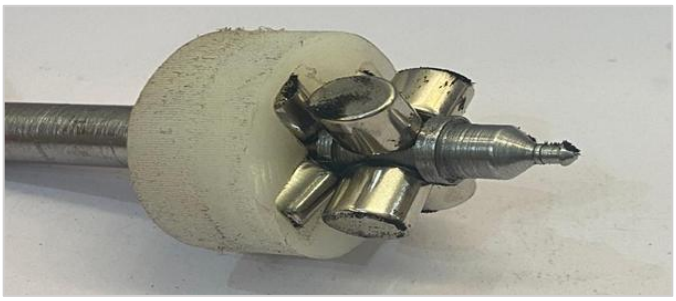

Figure 7: The final form finishing tool

Magnetic abrasive particles are the key ingredient in this finishing technique because they are responsible for removing the fine surface layer and achieving a smooth surface finish. They vary widely and are of different types depending on the need for which they are used. In this regard, the choice of the type of abrasive material greatly affects the finishing performance due to the difference in physical, chemical, and mechanical properties of each type [27]. In this study, a hybrid particle mixture was developed by preparing a two-component abrasive mixture consisting of silicon carbide (SiC) and tungsten carbide (WC) for their high hardness and wear resistance, as well as iron filings (Fe) to enhance the magnetic response. Moreover, acrylic resin was used as a binder, producing a homogeneous, grindable paste. More specifically, the components were mixed in the proportions studied: SiC 20%, WC 20%, and Fe 60%. This ratio plays a significant role in determining the processing and

finishing performance. The mixing ratio varies based on the desired properties of the intended application and the materials used. These ratios must be carefully considered and balanced, as they are a key factor influencing grinding performance and the resulting improvement [28]. Figure 8 EDX/SEM analysis of the magnetic–abrasive mixture (this work), a) SEM micrograph after bonding (scale bar: 500 µm; accelerating voltage 30 kV; magnification 250×; working distance 28.2 mm; detector ETD), b) Elemental distribution maps (W–L, Fe–K, C–K, Si–K); each panel shows a 500 µm scale bar; color bars indicate relative intensity (a.u.), c) EDX spectrum of the selected area with characteristic peaks of C, Fe, W, and Si (X-axis: Energy (keV); Y-axis: Counts (a.u.). Figure 9 SEM image of the magnetic abrasive grains after bonding and grinding the magnetic abrasive grains to show morphology and irregular particle shapes that improve cutting and finishing efficiency during MAF operations.

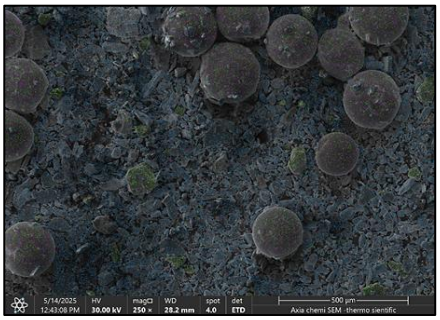

(a) The EDX analysis that shows the distribution of particles

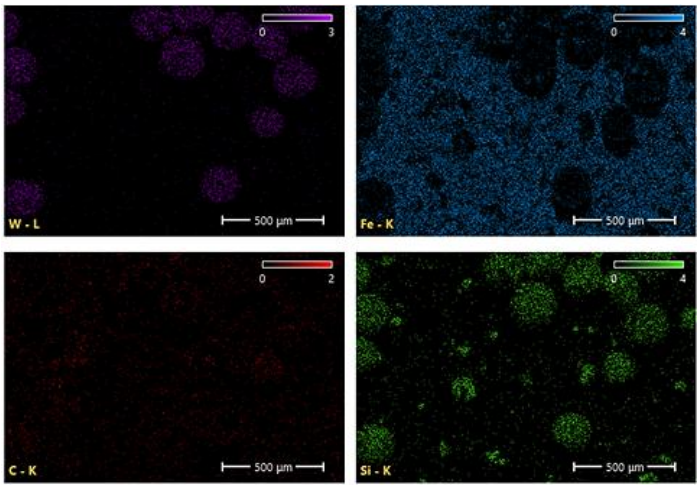

(b) The surface structure of the particles and how the elements are distributed

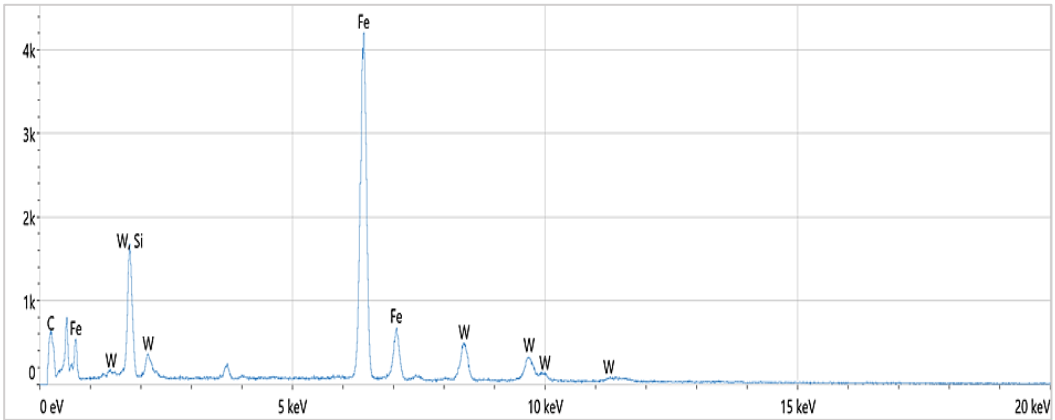

(c) The EDX analysis that shows the hybrid mixture and the elements

Figure 8: EDX/SEM analysis of the magnetic-abrasive mixture (this work) a) SEM micrograph after bonding (scale bar: 500 µm; accelerating voltage: 30 kV; magnification: 250×; working distance: 28.2 mm; detector: ETD) b) Elemental distribution maps (W–L, Fe–K, C–K, Si–K); each panel shows a 500 µm scale bar; color bars indicate relative intensity (a.u.), and c) EDX spectrum of the selected area showing characteristic peaks of C, Fe, W, and Si (x-axis: energy, keV; y-axis: counts, a.u.)

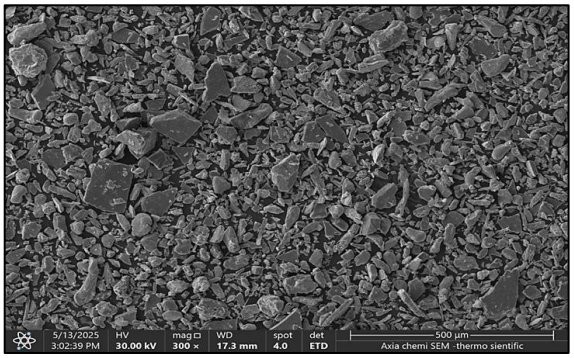

Figure 9: The SEM examination of the magnetic abrasive grains

Characterization of the EDM-processed and MAF-finished surfaces was performed using a scanning electron microscope (SEM) equipped with energy-dispersive X-ray spectroscopy (EDX). Specimens were ultrasonically cleaned in ethanol, air-dried, and sputter-coated with a ~10 nm conductive layer (Au/Pd or carbon, as appropriate) to suppress charging; the presence of the coating was considered when interpreting EDX spectra. SEM imaging was carried out in high-vacuum at an accelerating voltage of 10–15 kV and a working distance of approximately 8–12 mm, with beam current/spot size tuned to optimize contrast while minimizing charging and beam damage. For each condition, at least three non-overlapping fields were recorded at representative magnifications (~200×, 500×, 1000×, and higher when required), with scale bars reported; wherever feasible, the same regions were imaged before and after finishing to enable direct comparison. Elemental analyses were obtained with an SDD-type EDX detector using a live time of ~60 s per spectrum and maintaining dead time below 30%; point spectra, area scans, and elemental maps were acquired on representative regions. Quantification employed ZAF corrections with background subtraction and peak deconvolution, and results are reported as weight percent (mean ± SD, n = 3). Under these conditions, the practical detection limit was ~0.3–0.5 wt%. The SEM/EDX study was used to (i) assess the presence and thickness reduction of the EDM recast layer, (ii) document changes in burr density and surface-height homogeneity after MAF, and (iii) detect possible embedding of abrasive residues (e.g., SiC/WC), ferrous debris, and oxide formation associated with EDM and subsequent finishing.

Based on the obtained results, the tool rotation speed, the feed rate, and the abrasive particle size were found to be the three primary operational parameters that affect the effectiveness of the magnetic finishing (MAF) process. These parameters were identified for this study with three third-level selections. The Taguchi method was employed using an L9 (3^3) matrix, which comprised nine experiments with various sets of variables, to maximize the number of experiments while ensuring coverage of potential variations. Table 2 shows the design of the finishing experiments conducted.

Table 2: The design of the finishing experiments

No.	Feed rate (mm/min)	Spindle speed (rpm)	Particle size (µm)
1	35	300	200
2	35	500	300
3	35	750	600
4	70	300	300
5	70	500	600
6	70	750	200
7	90	300	600
8	90	500	200
9	90	750	300

After completing the previous stages and adjusting the variable levels, we are ready to begin the finishing process. In this regard, the finishing stage requires the use of a three-axis machine to perform finishing with high precision. Since the shape is not flat and contains a degree of complexity, a CNC machine was chosen to perform the finishing. This selection was also made because, in the initial stages of the practical aspect, the CNC machine was used to manufacture the shapes. Since the codes and operating programs are the same, this step facilitates the finishing process. Before commencing the finishing operations, the starting point was determined by zeroing in the finishing tool relative to the work sample to ensure accuracy. This step was carried out using a zeroing machine whose operating principle is that when the tool encounters the work sample, a signal is given by turning on a light. At this point, the position is determined, and a gap is created to represent the space that will be filled with abrasive particles. After finishing, the samples are tested in the same manner as before, after being processed with the EDM machine. To avoid repetition, this point is not reiterated here.

Repetition and measurement protocol. A Taguchi L9 orthogonal array was used for both EDM and MAF, yielding nine conditions per stage (9 EDM and 9 MAF). Each condition was performed with three independent replicates (n = 3). For EDM, machining time and specimen mass before/after machining were recorded for each replicate to compute the metal removal rate (MRR). Surface roughness (SR) was measured by 3D laser scanning at three distinct locations on each specimen; at each location, three repeated scans were acquired (3 × 3 = 9 readings per specimen). For each condition, we report mean ± standard deviation across replicates, and figures display error bars as SD (n = 3).

4. Results and discussion

4.1 The electrical discharge machining results

Table 3 presents the most significant results obtained from the machining process using EDM. Moreover, Figure 10 shows Surface examination results at different current values using laser scanning and SEM techniques, which show some images that occurred after operating the surface design samples using laser technology, along with the corresponding roughness diagrams. It also shows the electron microscope images of the samples after machining them with an electric spark-cutting machine, without any subsequent finishing, (a) Examination at 24 A: (1) Laser scanning results showing surface protrusions and roughness profile, (2–4) SEM images at different magnifications. (b) Examination at 36 A: (1) Laser scanning results with roughness profile, (2–4) SEM images at different magnifications. (c) Examination at 42 A: (1) Laser scanning results with roughness profile, (2–4) SEM images at different magnifications.

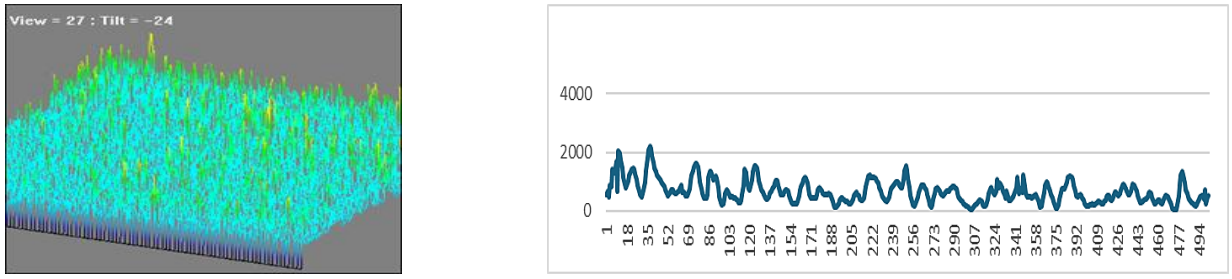

1. The result of the laser scanning technique examination

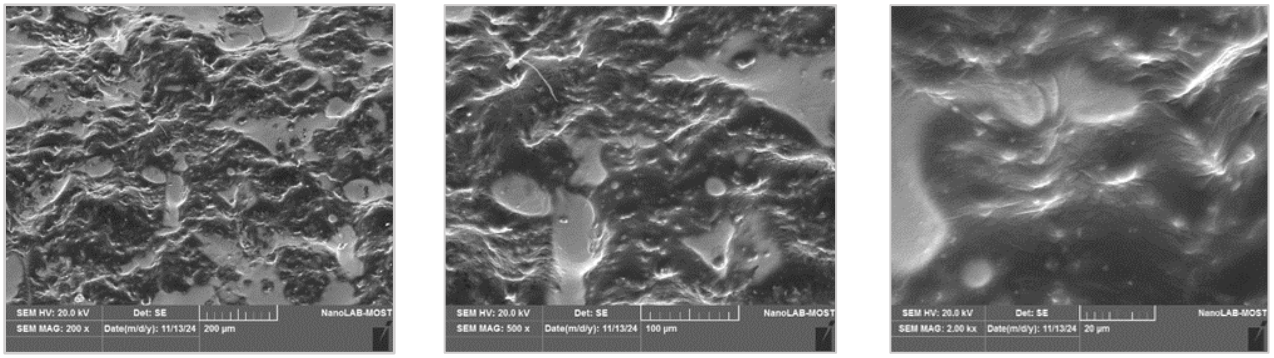

2. SEM tests with scale bar 200 µ **3. SEM tests with scale bar 100 µ** **4. SEM tests with scale bar 20 µ**

(a) A sample examination that was carried out at 24 A current

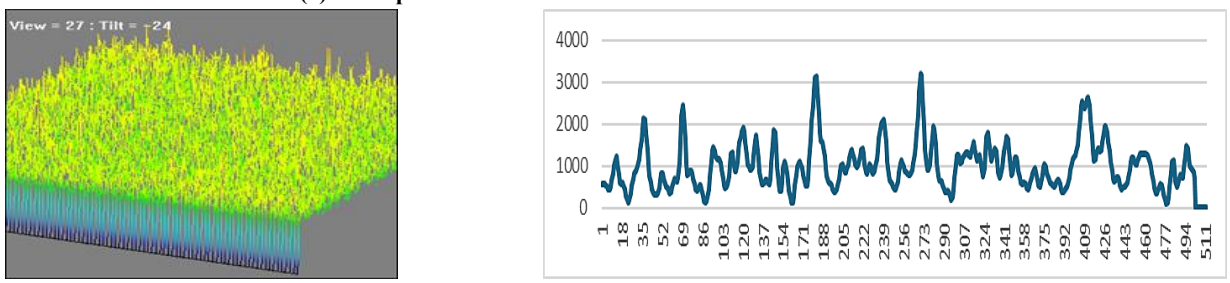

1. The result of the laser scanning technique examination

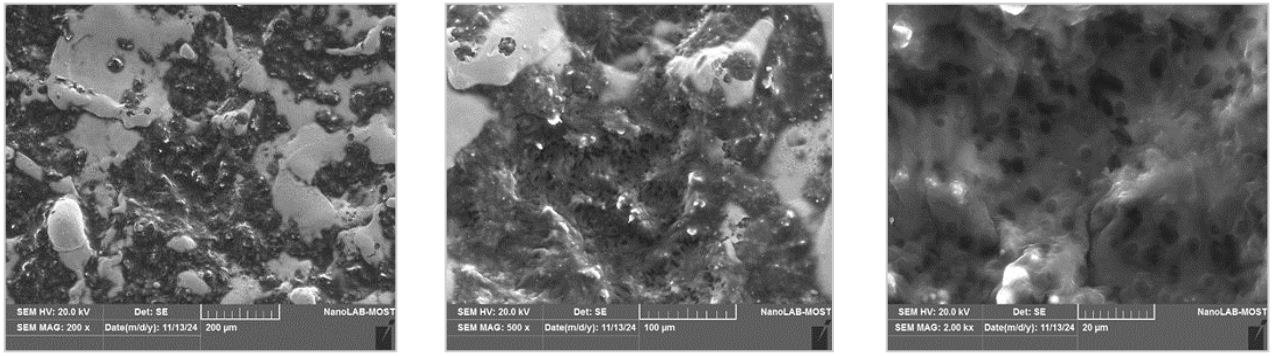

2. SEM tests with scale bar 200 µ **3. SEM tests with scale bar 100 µ** **4. SEM tests with scale bar 20 µ**

(b) A sample examination that was carried out at 36 A current

Figure 10: Surface examination after EDM (no finishing) at three currents. For each current, panel (1) shows the laser-scanning 3D height map and line-profile roughness plot (X: Lateral position (index/mm); Y: Height (µm/a.u.), followed by (2-4) SEM micrographs at increasing magnifications (scale bars: 200, 100, 20 µm): (a) 24 A; (b) 36 A; (c) 42 A

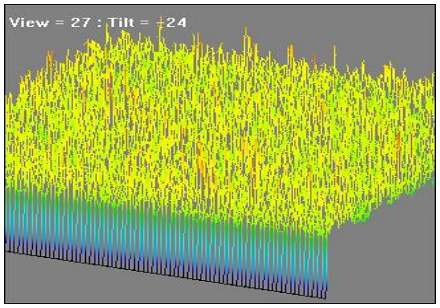

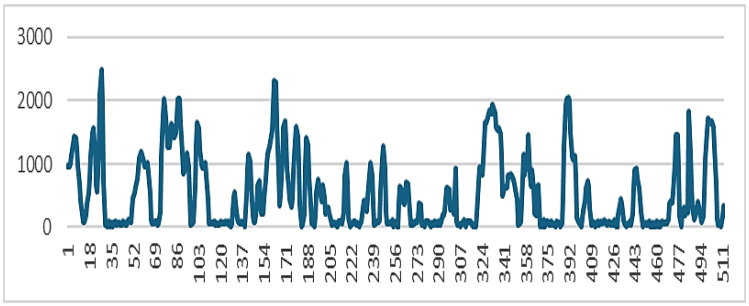

1. The result of the laser scanning technique examination

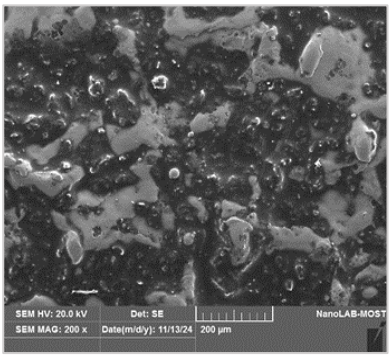

2. SEM tests with scale bar 200 µ

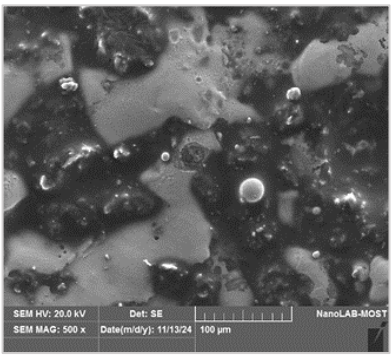

3. SEM tests with scale bar 100 µ

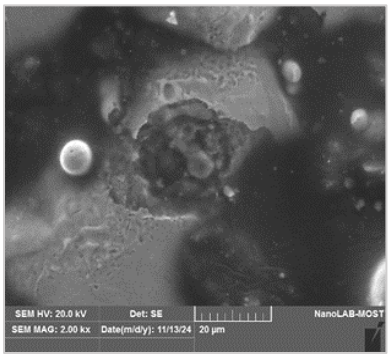

4. SEM tests with scale bar 20 µ

(c) A sample examination that was carried out at 42 A current

Figure 10: Continued

Table 3: The results of the models using EDM

No.	Current	Ton	Gap	Time (min)	(MRR) (mm³/min)	(Ra) (µm)
1	24	150	5	19	12.847	11.6674
2	24	200	8	16	13.993	11.9169
3	24	300	10	14	16.428	12.6501
4	36	150	8	12	17.974	13.173
5	36	200	10	11	19.0284	13.9912
6	36	300	5	9	19.9722	14.308
7	42	150	10	11	20.7086	14.8795
8	42	200	5	9	22.3175	15.0036
9	42	300	8	7	25.1024	15.437

At this stage, the results are analyzed according to the table extracted from the practical experiments. The table of the results for the electrical discharge machining process shows that increasing the current (from 24 to 42 A), with all other variables kept constant, results in a significant increase in the metal removal rate (from 12.847 to 25.1024 mm³/min). This increase is accompanied by surface deformation, as the surface roughness values also increase from 11.6674 to 15.437 µm. Increasing the current from 24 to 42, a raised the mean MRR from 14.42 to 22.71 mm³/min (+57%), while the mean Ra increased from 12.08 to 15.11 µm (+25%), evidencing the productivity quality trade-off. At 24 A, extending Ton from 150 to 300 µs increased MRR from 12.847 to 16.428 mm³/min (+27.9%) and Ra from 11.6674 to 12.6501 µm (+8.4%). Higher Ip and Ton increase the discharge energy ($E \propto Ip \cdot V \cdot Ton$), enlarging the crater volume and the recast layer; consequently, MRR rises at the cost of higher Ra. SEM observations agree with these trends (more re-solidified debris and micro-craters at higher Ip/Ton).

Figure 11, effect of discharge current and pulse duration on the material removal rate (MRR) and surface roughness (SR). The results show that increasing the current and extending the pulse duration led to a significant rise in the MRR (from 12.847 to 25.1024 mm³/min), accompanied by a gradual increase in SR (from 11.6674 to 15.437 µm), indicating the trade-off between higher productivity and surface quality.

In this work, the effect of the working gap did not appear to significantly affect the process performance compared to the effect of the current and the pulse duration. In fact, small gaps helped achieve better spark distribution and a more uniform surface, while large gaps led to a dispersion of the spark energy.

In this context, the SEM and the laser data analysis visually confirmed these results, showing that samples operated at lower currents had less angular surfaces than those operated at higher currents and longer pulse durations. The reliability of the laser scanning data was also supported by the SEM images, which revealed fine cracks and prominent lines resulting from the electrical actuation process.

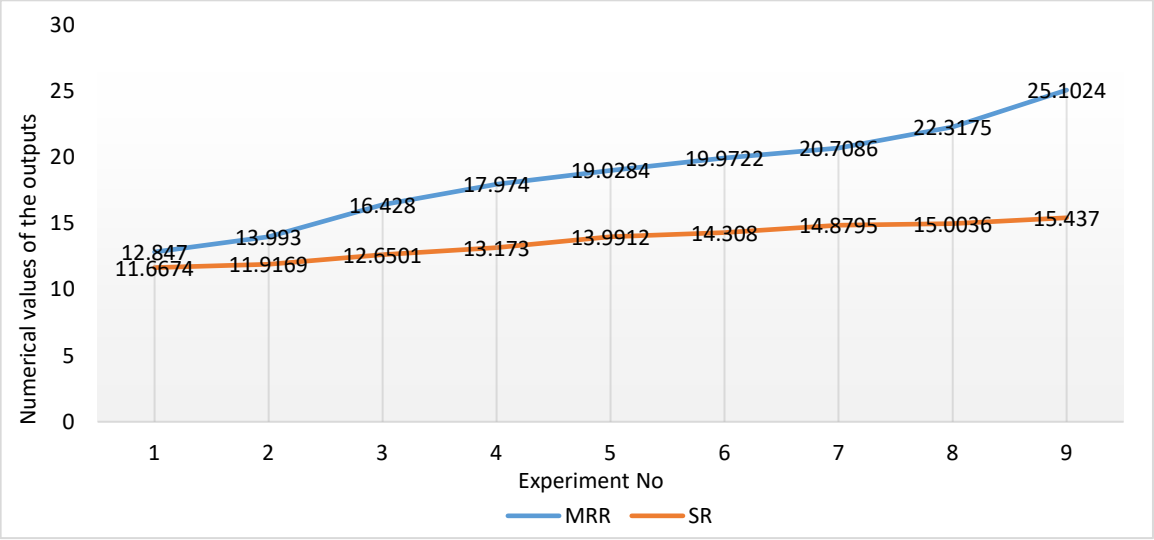

Figure 11: The effect of the current and the pulse time on the MRR and the SR

To this end, the authors in [23], and [29], revealed that the current serves as the main determining factor influencing the metal removal rate and the roughness, together with the tool wear. Therefore, high current levels yield optimal results in all three areas. The length of the pulse time directly correlates with the surface quality and the removal rate, creating more surface defects and tool failures, although it promotes increased material removal. In addition, the electrical gaps have a direct impact on the tool wear and the metal removal rate, but they remain a weaker influence than other factors. The process is affected by the distinctive properties that different materials present. In [24] and [30], the research analyzed several types of variables. It concluded that the low energy resulting from the low current and the shortest spark operation time led to improved surface quality and reduced the roughness of the product. The research highlighted the significance of the shape used for cutting tools, noting that the best removal rate is achieved with tools that contain curves and are circular, followed by square, triangular, and diamond-shaped tools. This paper examined the response of the electric spark cutting process to various variables, including tool dimensions and electrical measures, as well as pulse timing, material characteristics, and fluid control. Operating parameters, including current and voltage, together with pulse time, control the quantity of metal removal and the level of surface roughness. The process of metal removal improves with elevated operating parameters, but surface quality and precision deteriorate. Particularly, the material behaves differently when subjected to mechanical stress, and fluid operations serve both to cool the working region and extract dissolved particles [25,31]. The research presented a new method for examining surface roughness, based on the color index of the workpiece layers, obtained from laser reflection micrographs instead of traditional grayscale images. The practical aspect demonstrates that when the laser is reflected, the scattered rays are detected from the surface containing high protrusions (surface roughness). The results were then photographed and interpreted as layers of different colors, depending on the surface roughness. It was possible to collect high-resolution image data of about 90% compared with traditional surface roughness measurement methods, and the results of these experiments are very practical for complex and precise shapes that are difficult to examine [32].

The Taguchi method is used to analyze the influence of operational variables on the process performance and efficiency. In this section, the effect of the three variables, namely the electric current, the pulse time (Ton), and the gap between the two electrodes, on the metal removal rate and the surface roughness will be analyzed, and the effect of each factor will be determined over the others. According to the results of the linear regression analysis, the electrical current had the greatest impact on both MRR and SR. In fact, lowering the current to 24 A considerably improved roughness and decreased MRR ($P < 0.05$). The 150 µs pulse duration significantly impacted both responses. However, the gap variation had no discernible impact ($P > 0.05$). If $P < 0.05$, the effect is significant (reliable). If $P > 0.05$, the effect is not statistically significant (possibly due to chance). Table 4 presents the results of the linear regression coefficients for the metal removal rate, while Table 5 displays the linear regression results for the surface roughness.

Table 4: Linear regression model coefficients for the MRR

Factor	Regression Coefficient	Standard Error of Coefficient	T-value	P-value
Constant	18.7079	0.2429	77.011	0.0
Current 24	-4.2852	0.3435	-12.473	0.006
Current 36	0.2836	0.3435	0.826	0.496
T-on 150	-1.5314	0.3435	-4.458	0.047
T-on 200	-0,2616	0.3435	-0.761	0.526
Gap 5	-0.3290	0.3435	-0.958	0.439
Gap 8	0.3152	0.3435	0.918	0.456
Model Summary	S	R-sq	R-sq (adj)	
	0.7288	99.1%	96.5%	

Table 5: Linear regression model coefficients for the SR

Factor	Regression Coefficient	Standard Error of Coefficient	T-value	P-value
Constant	13.6696	0.03038	449.978	0.0
Current 24	-1.5915	0.04296	-37.045	0.001
Current 36	0.1544	0.04296	3.595	0.069
T-on 150	-0.4297	0.04296	-10.001	0.010
T-on 200	-0.0324	0.04296	-0.754	0.529
Gap 5	-0.0100	0.04296	-0.232	0.838
Gap 8	-0.1607	0.04296	-3.740	0.065
Model Summary	S	R-sq	R-sq (adj)	
	0.09114	99.9%	99.6%	

Table 6: Analysis of variance (ANOVA) for the MRR

Source	DF	Seq SS	Adj SS	Adj MS	F	P
Current	2	103.369	103.369	51.6847	97.31	0.010
T-on	2	16.885	16.885	8.4424	15.9	0.059
Gap	2	0.623	0.623	0.3117	0.59	0.630
Residual Error	2	1.062	1.062	0.5311		
Total	8	121.940				

Table 7: Analysis of variance (ANOVA) for the SR

Source	DF	Seq SS	Adj SS	Adj MS	F	P
Current	2	13.8656	13.8656	6.93282	834.71	0.001
T-on	2	1.1975	1.1975	0.59875	72.09	0.014
Gap	2	0.1651	0.1651	0.08254	9.94	0.091
Residual Error	2	0.0166	0.0166	0.00831		
Total	8	15.2449				

At this stage, an ANOVA analysis of MRR and SR was performed by presenting the results of the two tests extracted from the Minitab 18 application. Tables 6 and 7 illustrate the analysis of variance for both the metal removal rate and the surface roughness.

ANOVA percent contributions (from Seq SS) confirm factor ranking. For MRR: Current 84.8%, Ton 13.9%, Gap 0.5%. For SR: Current 91.0%, Ton 7.9%, Gap 1.1%.With F values (97.31 for MRR and 834.71 for SR) being highly significant ($P < 0.05$), the analysis of variance (ANOVA) results demonstrated that the electric current had the greatest impact on both the MRR and the SR. In contrast, the effect of the electrode gap was small and negligible ($P > 0.05$), whereas the pulse time also demonstrated a moderate to strong effect ($F = 15.9$ for MRR and $F = 72.09$ for SR).

One of the fundamental tools in the Taguchi methodology for analyzing the effect of variables is the signal-to-noise (S/N) ratio. This ratio aims to maximize performance and minimize unwanted variations. By applying the S/N analysis, the responses can be evaluated based on the "larger is better" criterion for the MRR and the "smaller is better" criterion for the Ra. Tables 8 and 9 show the signal-to-noise ratio results for both the MRR. Figure 12 Main-effects plot of the signal-to-noise (S/N) ratio for MRR (larger-is-better): panels show factor levels for Current (A), Pulse duration (µs), and Gap (mm). Figure 13 Main-effects plot of the S/N ratio for SR (smaller-is-better): panels for Current (A), Pulse duration Ton (µs), and Gap (mm). Table 1 Signal-to-noise (S/N) ratio for the MRR. For each figure, Y-axis: S/N ratio (dB); X-axis (each panel): factor level with units.

Table 8: Signal-to-noise (S/N) ratio for the MRR

Level	Current	Ton	Gap
1	23.14	24.53	25.05
2	25.56	25.16	25.34
3	27.10	26.10	25.41
Delta	3.96	1.57	0.36
Rank	1	2	3

Table 9: Signal-to-noise (S/N) ratio for the SR

Level	Current	Ton	Gap
1	-21.63	-22.39	-22.66
2	-22.81	-22.65	-22.56
3	-23.58	-22.97	-22.80
Delta	1.95	0.58	0.24
Rank	1	2	3

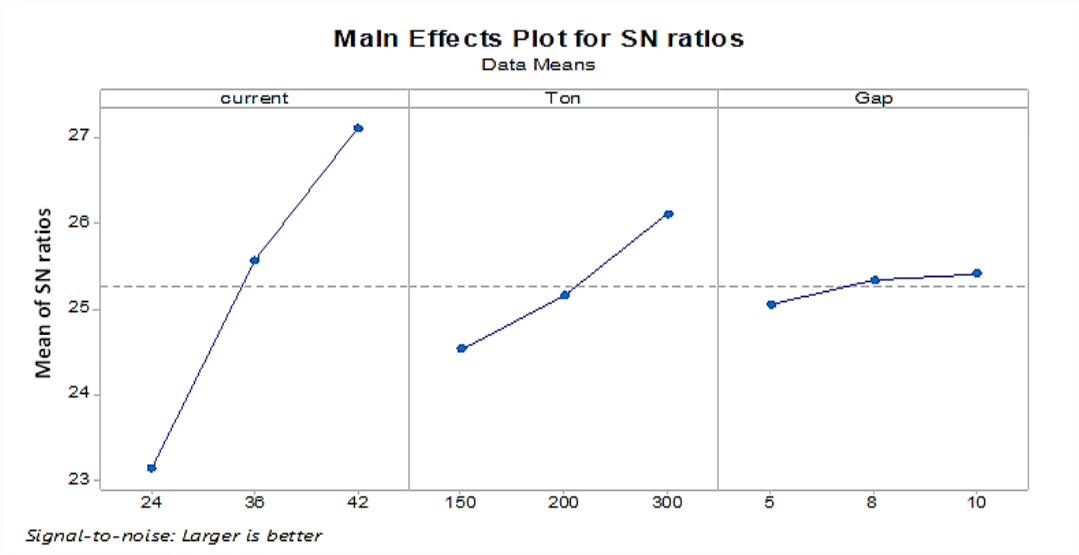

Figure 12: The S/N main effects plot for the MRR

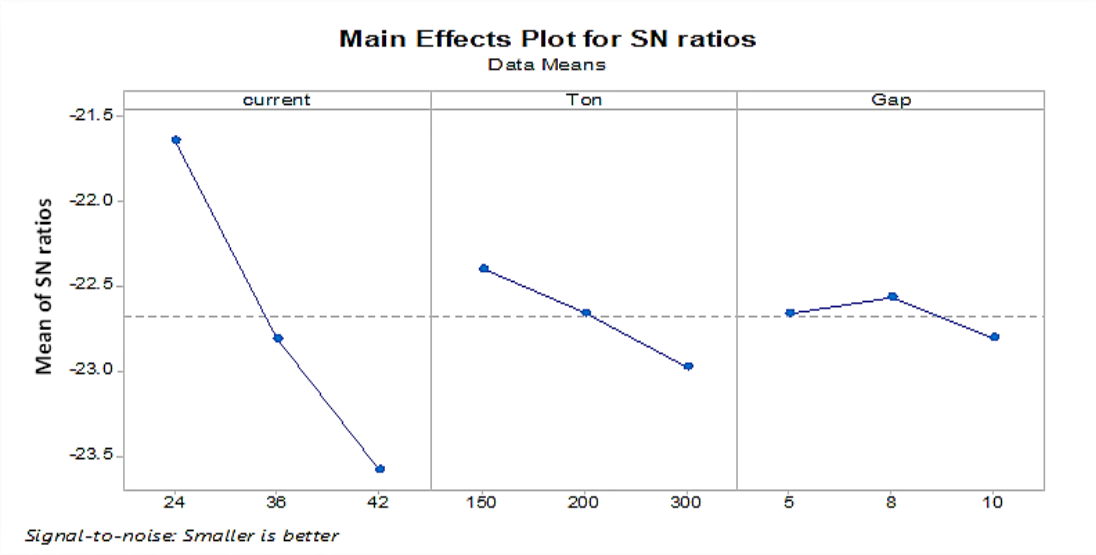

Figure 13: The S/N main effects plot for the SR

The signal-to-noise ratio analysis confirms the ranking of variables in order of importance, with the current as the most influential parameter, with Δ = 3.96 for the MRR, and Δ = 1.95 for the SR. The pulse duration is second, followed by the gap.

Based on the results of a linear regression analysis derived from experimental values and analyzed using the Taguchi application, equation models were constructed for both the metal removal rate and the surface roughness. These models aim to provide a mathematical means for estimating the response level based on the values of the variables. The first level of each factor was chosen as a reference for the other levels, and the other levels were expressed within the model.

The following Equations (1,2) is used to estimate the predictive values of the MRR, based on the regression coefficients obtained from the analysis:

$$MRR = 18.7079 - 4.2852(Current_{(}24_{)}) + 0.2836(Current_{(}36_{)}) - 1.5314(Ton_{(}150_{)}) - 0.2616(Ton_{(}200_{)}) - 0.3290(Gap_{(}5_{)}) + 0.3152(Gap_{(}8_{)}) \quad (1)$$

The following equation is used to estimate the predictive values of the SR:

$$Ra = 13.6696 - 1.5915(Current_{(}24_{)}) + 0.1544(Current_{(}36_{)}) - 0.4297(Ton_{(}150_{)}) - 0.0324(Ton_{(}200_{)}) - 0.0100(Gap_{(}5_{)}) - 0.1607(Gap_{(}8_{)}) \quad (2)$$

Models use level-coded indicator variables (level 1 as reference). Predicted values closely matched the experiments with a mean error = 1.81% for MRR and 0.30% for SR (Table 10; Figure 14).

Table 10 shows the actual experimental values and the values predicted from the linear regression equations for both the metal removal rate and the surface roughness.

Table 10: Actual and predicted values of the MRR and the SR

No.	Actual MRR	Actual SR	Predicted MRR	Predicted SR	MRR Error%	SR Error %
1	12.847	11.6674	12.5623	11.6385	2.2161	0.24769
2	13.993	11.9169	14.4763	11.8851	3.4539	0.26684
3	16.428	12.6501	16.2294	12.7108	1.2089	0.47983
4	17.974	13.173	17.7754	13.2337	1.1049	0.46079
5	19.0284	13.9912	18.7437	13.9623	1.4962	0.20655
6	19.9722	14.308	20.4555	14.2762	2.4198	0.22225
7	20.7086	14.8795	21.1919	14.8477	2.3338	0.21371
8	22.3175	15.0036	22.1189	15.0643	0.8899	0.40457
9	25.1024	15.437	24.8177	15.4081	1.1342	0.18721

The predictive accuracy of the regression equations was evaluated by comparing the actual and the predicted values (Table 10 and Figure 14). More specifically, the predicted values closely matched the actual experimental data, with low average prediction errors of 1.81% for the MRR and 0.30% for the SR. This outcome demonstrates the model's reliability in estimating future responses. Figure 14. Comparison between actual and predicted values of material removal rate (MRR) and surface roughness (SR). The predicted results obtained from the regression equations closely follow the experimental values, with low prediction errors (1.81% for MRR and 0.30% for SR). This confirms the reliability of the developed model in estimating future responses.

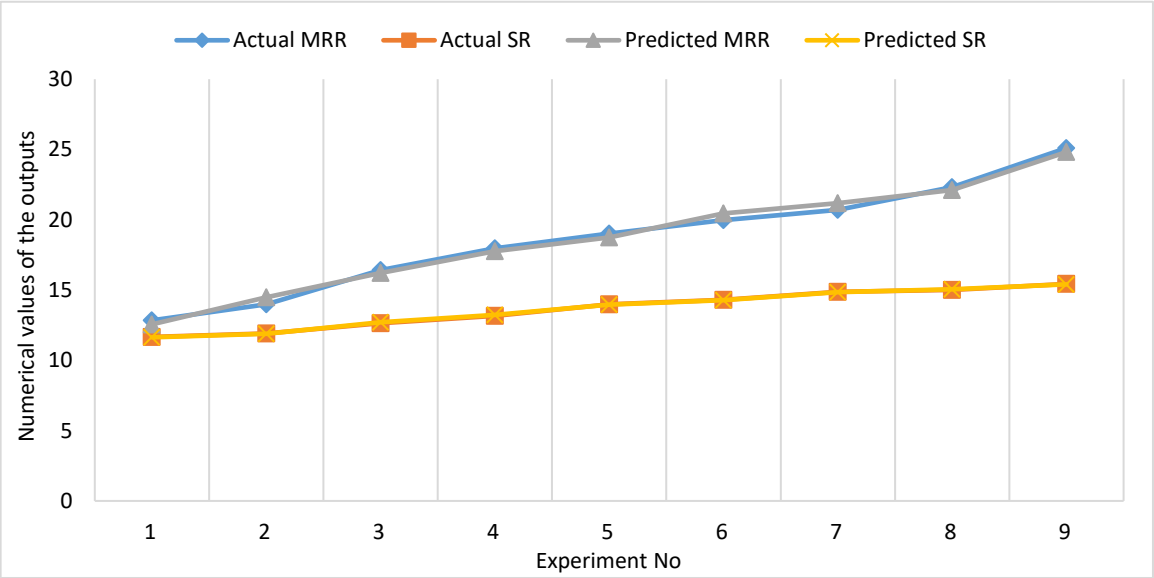

Figure 14: A comparison between actual and predicted values

Any study that seeks to balance productivity and surface quality must include a multi-objective optimization phase, particularly in non-traditional processes such as EDM. The balance or combination of several goals, such as the simultaneous removal of metal and the reduction of roughness, is not considered by Taguchi analysis, which is used to ascertain the effect of each variable independently on the responses. As a result, using the Grey Relational Analysis offers a useful method for combining disparate goals into a single index. This analysis can be used to select the optimal machining experience that yields balanced performance, enhancing the quality of the finished product, decision accuracy, and process efficiency. In particular, this technique can transform more than one physical objective into a unified criterion against which the optimum level of the experiment can be evaluated. In this regard, the highest GRG value represents the optimal solution that can achieve the best productivity while maintaining quality. Table 11 shows the analysis of the results and the determination of the optimum level.

Table 11: The optimum level of the surface sample

No.	S/N ratio (SR)	S/N ratio (MRR)	Normalization S/N (SR)	Normalization S/N (MRR)	Coefficients of Grey (SR)	Coefficients of Grey (MRR)	GRG
1	-21.6	22.176	0	1	0.333	1	0.666
2	21.8	22.912	0.956	0.872	0.921	0.796	0.858
3	22.1	24.311	0.964	0.632	0.934	0.576	0.755
4	22.5	25.092	0.972	0.498	0.947	0.499	0.723
5	22.9	25.588	0.982	0.413	0.965	0.464	0.712
6	23.2	26.002	0.988	0.341	0.977	0.431	0.704
7	23.5	26.301	0.994	0.287	0.988	0.412	0.701
8	23.7	26.291	1	0.175	1	0.377	0.688
9	24	27.99	1.006	0	0.3311	0.333	0.332

The second experiment with surface design was selected and adopted as a sample for quality improvement in the next finishing process, as this experiment achieved the best balance between production efficiency and surface quality. After the machining phase and optimization, nine samples were manufactured, all of which were run under the same experimental conditions as those of the second surface design experiment. The finishing process is performed using three variables (tool rotation speed, feed speed, and abrasive particle size) at three levels to determine the effect of each variable individually, as well as the combined effect of these variables on surface quality. Figure 10 shows the sample on which the finishing operations are carried out with a roughness level of 11.9169 µm.

4.2 The magnetic abrasive finishing result

Table 12 presents the most significant results obtained from the machining process using the MAF. Figure 15 Laser inspection results and SEM analysis of the surface design samples after finishing with MAF technology a) Sample examined at a feed rate of 35 mm/min: (1) laser scanning examination showing surface protrusions with roughness diagram; (2–4) SEM images at different magnifications b) Sample examined at a feed rate of 70 mm/min: (1) laser scanning examination with roughness diagram; (2-4) SEM images at various magnifications, and c) Sample examined at a feed rate of 90 mm/min: (1) laser scanning examination with roughness diagram; (2–4) SEM images at different magnifications.

Table 12: The results of the first pass finishing process

No.	Federate (mm/min)	Tool rotation speed (rpm)	Particles size (µm)	New Roughness (Ra) (µm)	Δ Ra	Improvement ratio
1	35	300	200	4.836	7.0766	59.41%
2	35	500	300	4.29	7.6226	64.02%
3	35	750	600	4.329	7.5836	63.68%
4	70	300	300	5.811	6.1016	51.24%
5	70	500	600	5.428	6.4846	54.45%
6	70	750	200	5.1943	6.7183	56.41%
7	90	300	600	6.7492	5.1634	43.38%
8	90	500	200	6.3483	5.5643	46.74%
9	90	750	300	6.2873	5.6253	47.26%

MAF reduced Ra from 11.9169 µm to ≈4.29 µm (64.02%). Improvement decreased with increasing feed rate (≈59–64% at 35 mm/min vs. <48% at 90 mm/min), while a mid-range speed (500 rpm) balanced brush stability and kinetic energy. Particle size 300 µm yielded the most uniform reduction; 600 µm risked scratching/instability, whereas 200 µm was less energetic.

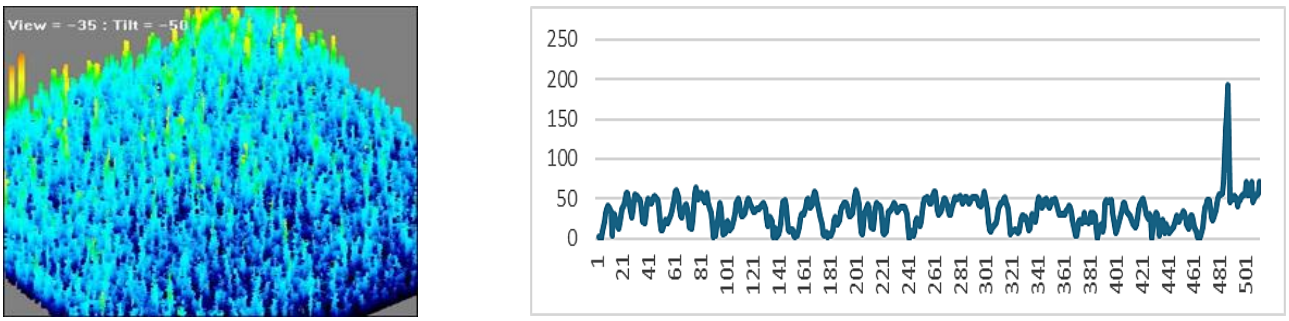

1. The result of the laser scanning technique examination

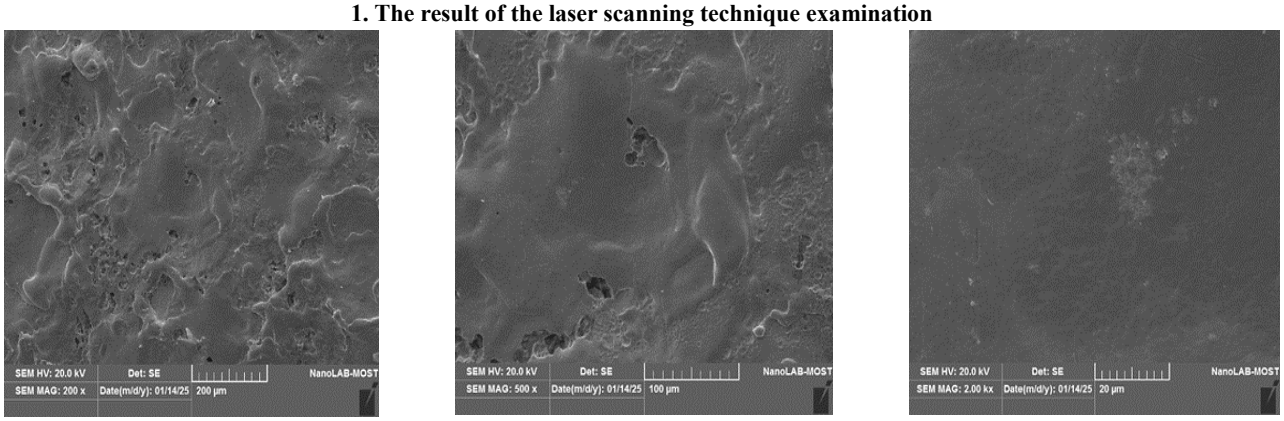

2. SEM tests with scale bar 200 µ **3. SEM tests with scale bar 100 µ** **4. SEM tests with scale bar 20 µ**

(a) A sample examination carried out at 35 mm/min federate

Figure 15: Laser-scanning outputs and SEM micrographs after MAF. For each feed rate (35, 70, 90 mm/min): (1) 3D map + line profile (X: Lateral position; Y: Height (µm/a.u.)), (2–4) SEM micrographs (scale bars: 200, 100, 20 µm) a) 35 mm/min; b) 70 mm/min, and c) 90 mm/min

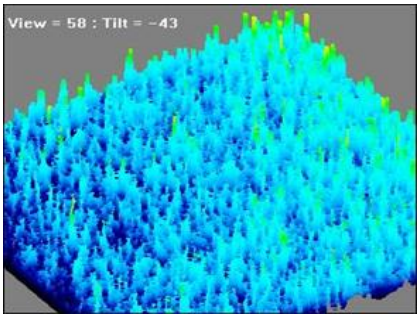

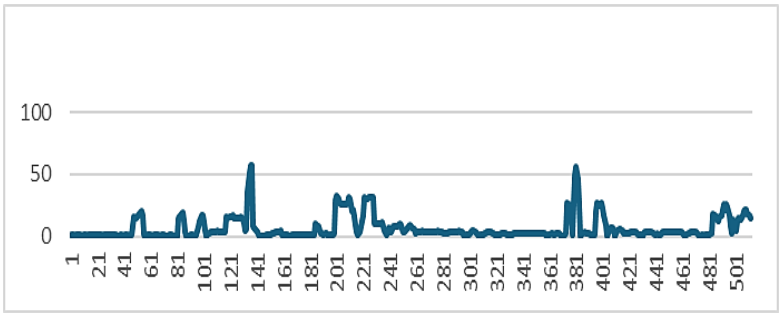

1. The result of the laser scanning technique examination

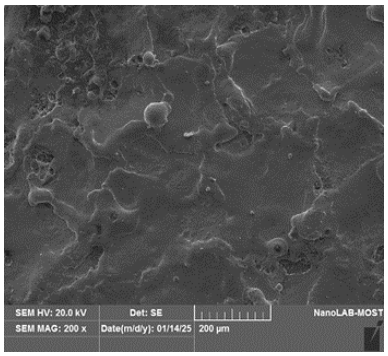

2. SEM tests with scale bar µ

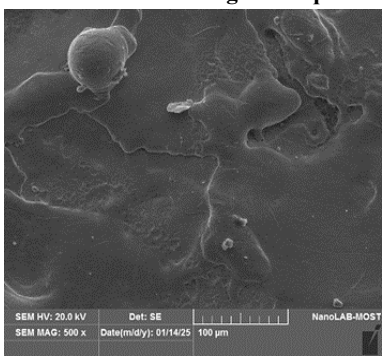

3. SEM tests with scale bar 100 µ

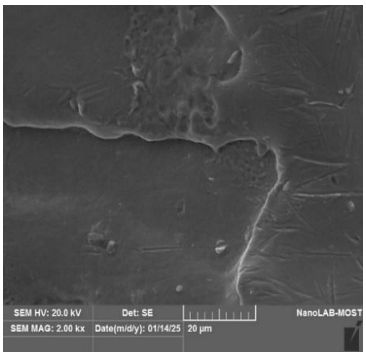

4. SEM tests with scale bar 20 µ

(b) A sample examination carried out at 70 mm/min federate

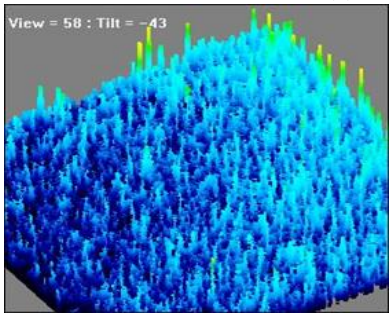

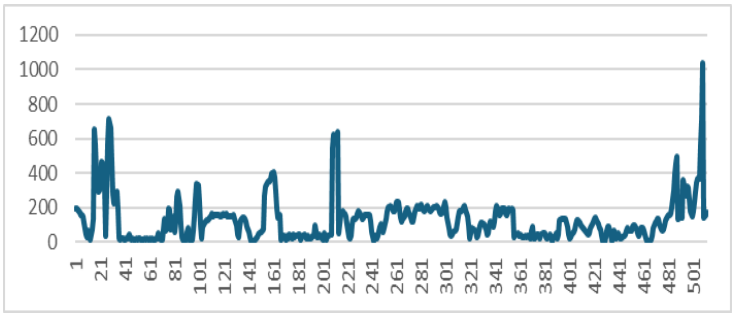

1. The result of the laser scanning technique examination

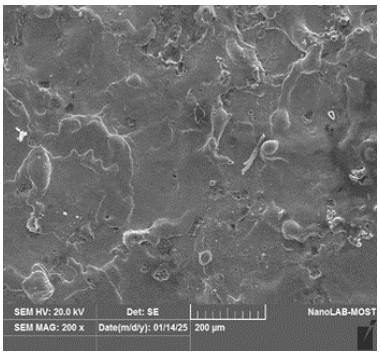

2. SEM tests with scale bar 200 µ

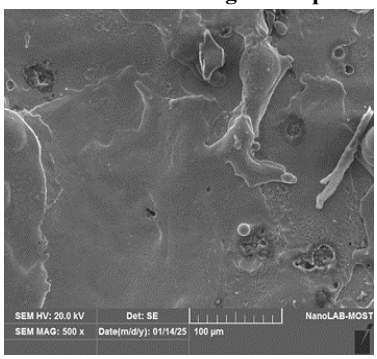

3. SEM tests with scale bar 100 µ

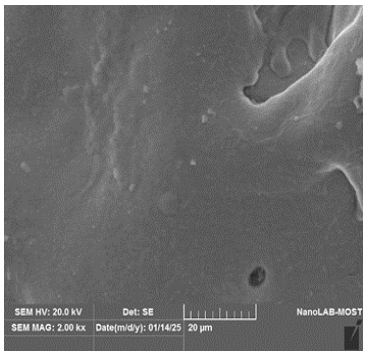

4. SEM tests with scale bar 20 µ

(c) A sample examination carried out at 90 mm/min federate

Figure 15: Continued

Table 12 of the results indicated that the finishing procedure was effective in improving surface roughness percentages. Particularly, the efficiency of roughness reduction was examined in relation to the feed speed, the tool rotation speed, and the abrasive particle size. In this context, the findings indicated an inverse relationship between the percentage of roughness improvement and the feed rate. Due to the short effective contact time between the particles and the sample surface, the percentage dropped to less than 48% at a high speed (90 mm/min), whereas the greatest improvement was obtained at a low speed (35 mm/min), ranging from 59.4 to 64%. On the other hand, it was found that a medium rotation speed (500 rpm) was optimal for achieving equilibrium between particle stability and kinetic energy in the magnetic field, which helped to improve the surface uniformly. However, the high speed (750 rpm) caused loss of magnetic stability and disruptions in particle distribution, which decreased performance efficiency. In fact, the best results were obtained in terms of uniform distribution and roughness reduction with medium-sized particles (300 µm). Large particles (600 µm) resulted in a loss of magnetic stability and

the potential for surface scratching or failure to reach microcavities. In contrast, small particles (200 µm) were ineffective because of their low energy.

After finishing, laser scanning and electron microscopy images confirmed a notable improvement in surface smoothness and the elimination of noticeable flaws, thereby strengthening the accuracy of the numerical results and demonstrating the effectiveness of the finishing procedure.

It is worth mentioning that the finishing stages and the effect of variables are not identical in all studies. They depend on the finishing conditions used, as the interaction of variables with each other affects the process's performance and depends on the level of surface roughness being finished [18]. However, there is some agreement between the results of this work and those of some previous studies. In [26], the research focused on examining the effect of tool development and certain variables on surface roughness. Some variables were selected, including the magnet speed (200, 400, 600, and 800 RPM) and the finishing time (0.5, 1.0, 1.5, and 2.0 hours). After conducting practical experiments, the effect of variables in the process was identified as follows: Surface roughness improves at medium speeds. Then, the roughness increased due to centrifugal forces. As for the effect of the finishing period, as it increases, there is a continuous decrease in surface roughness. The most important conclusions of the experiments are that the surface roughness improved by 76%, with the roughness reaching 96 nm. In [27], the effect of operational variables on the rough surface of the product during the MAF process was examined. The CNC_MAF process operated on aluminum, where the mixture of aluminum oxide abrasive particles, iron particles, and cleaning oil was kept to a rate of 5%. The parameters used are the rotation speed, ranging from 1000 to 2500 rpm, the feed rate, from 10 to 25 mm/min, and the number of process repetitions, from 3 to 9 times. The research demonstrated that the CNC MAF processes enable the highest accuracy in machine tools management and movement. The test results showed that the optimal operational settings achieved an rpm value of 1500, accompanied by a feed rate of 50 mm/min. The highest effective setting occurs when roughness decreases according to the number of revolutions in operation. The highest surface finish measurement of 0.04 mm occurred when the process revealed its optimal configuration. Moreover, the authors in [28], studied the magnetic finishing process, which depends mostly on the magnetic finishing tool rotation speed, the magnetic field intensity, and the workspace dimensions, as well as the abrasive particle weight and the iron particle ratio. Among the primary factors studied in the process were the rotational speed, which was the most influential variable, followed by the magnetized abrasive particle weight and the workspace dimensions, which significantly influenced the results at rates of (39.7, 32.74, and 22.87) %, respectively.

The Taguchi method and statistical analysis were employed to assess the impact of operational variables (feed speed, tool rotation speed, and abrasive particle size) on the efficiency of the finishing process and the reduction of surface roughness. The linear regression analysis was employed to determine the individual effects of each variable. Table 13 shows the results of the linear regression analysis of the means.

Table 13: Linear regression model coefficients for the SR

Factor	Regression Coefficient	Standard Error of Coefficient	T-value	P-value
Constant	5.47479	0.03238	169.061	0.0
Feed rate 35	-0.98979	0.0458	-21.612	0.002
Feed rate 70	0.00298	0.0458	0.0654	0.954
Rpm 300	0.32394	0.0458	7.073	0.019
Rpm 500	-0.11936	0.0458	-2.606	0.121
p.saize 200	-.0.01526	0.0458	0.333	0.771
p.size 300	-0.01202	0.0458	0.263	0.817
Model Summary	S	R-sq	R-sq (adj)	
	0.09715	99.7%	98.8%	

The results of the regression analysis showed that a feed speed of 35 mm/min was the most effective for extracting the lowest roughness (the highest improvement value) and was the most significant parameter in these experiments. In contrast, the tool rotation speed had a moderate effect on the process's effective performance, while the particle size was the least influential factor in these experiments.

To assess the level of the statistical influence of each factor, a variance analysis was performed using linear regression analysis. Table 14 displays the amount of variance for each factor, which helps determine the level.

Table 14: Analysis of Variance (ANOVA) for the SR

Source	DF	Seq SS	Adj SS	Adj MS	F	P
Feed rate	2	5.86046	5.86046	2.93023	310.46	0.003
Rpm	2	0.48313	0.48313	0.24156	25.59	0.038
p.size	2	0.00336	0.00336	0.00168	0.18	0.849
Residual Error	2	0.01888	0.01888	0.00944		
Total	8	6.36583				

The results of the analysis of variance showed that the feed rate factor has a p-value of 0.003, which is the most significant factor, followed by the rotation speed, which showed a medium inhibitory effect with a p-value of 0.038. Regarding the particle size, it did not exhibit a significant effect, indicating a weak role in improving the surface during this study. The signal-to-noise ratio represents the accuracy and stability of performance in response to varying levels of a changing variable. It is based on the

"bigger is better" criterion for response values. A standard is based on the amount of improvement, and hence, the greater the improvement, the better, as shown in Table 15.

Table 15: Signal-to-noise (S/N) ratio for the SR

Level	Current	Ton	Gap
1	-13.02	-15.19	-14.68
2	-14.76	-14.47	-14.63
3	-16.20	-14.34	-14.67
Delta	3.18	0.85	0.05
Rank	1	2	3

The extracted response tables confirm what was analyzed in the (S/N) ratio analysis. The factor whose level is the strongest and most decisive in determining the level of finishing process efficiency is the feed rate, followed closely by the rotation speed, which depends on other levels to produce the best results. Finally, the weakest influence is the particle size.

The regression analysis enables the derivation of the predictive equations that express the system's behavior and facilitate the calculation of the expected roughness for any combination of input factor levels. The final Equation (3) derived from the regression coefficient table to predict surface roughness was as follows:

$$Ra = 5.47479 - 0.98979(feedrate35) + 0.00298(feedrate70) + 0.32394(rpm300) - 0.11936(rpm500) - 0.01526(p.size200) - 0.01202(p.size300) \quad (3)$$

Table 16: Actual and predicted values of the SR

No.	Federate (mm/min)	Tool rotation speed (rpm)	Particles size (µm)	Actual SR	Predicted SR	SR Error %
1	35	300	200	4.836	4.79369	0.87
2	35	500	300	4.29	4.35362	1.49
3	35	750	600	4.329	4.30769	0.49
4	70	300	300	5.811	5.78969	0.37
5	70	500	600	5.428	5.38569	0.78
6	70	750	200	5.1943	5.25792	1.22
7	90	300	600	6.7492	6.81282	0.94
8	90	500	200	6.3483	6.32699	0.34
9	90	750	300	6.2873	6.24499	0.67

The results showed good convergence between the actual and the predicted values, reflecting the accuracy of the predictive model. The average difference between the values was small, supporting the validity of using the derived equation to estimate process performance within the range of variables used. The mean error value of the predictive values proved the accuracy and reliability of the results, reaching approximately 0.82%. Figure 16 Comparison between actual and predicted values of surface roughness (SR). The results demonstrate a very close agreement between experimental measurements and regression model predictions, with a prediction error of approximately 0.82%, confirming the accuracy and reliability of the developed model.

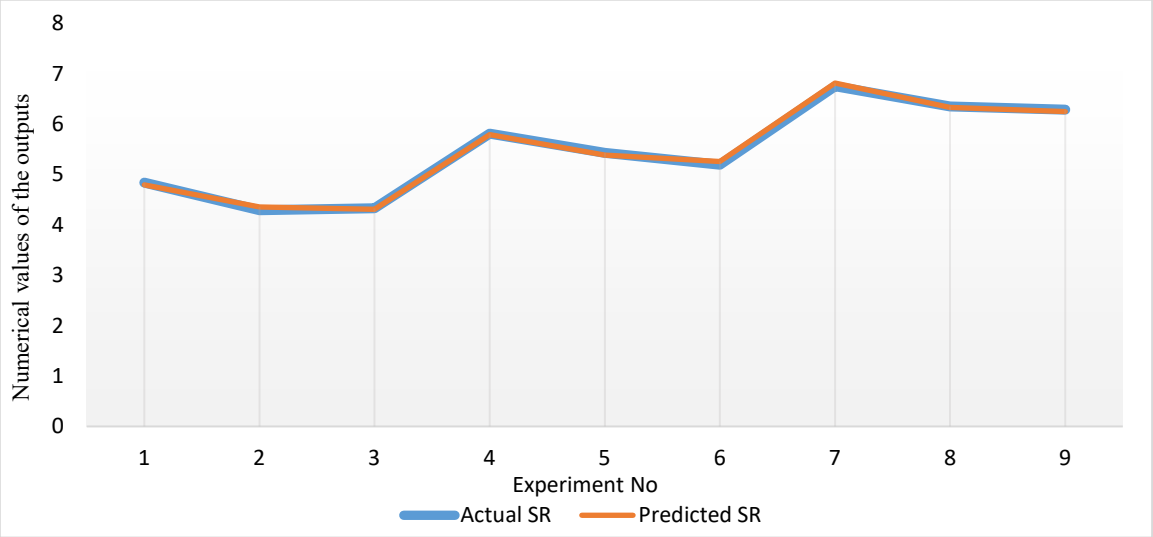

Figure 16: Comparison between actual and predicted values

The MAF finishing process proved to be highly effective in improving the surface roughness resulting from the electro-spark machining process. In particular, the process yielded remarkable improvement results, as the surface roughness decreased from 11.9169 µm to approximately 4.29 µm, representing a 64.02% improvement rate. This outcome demonstrates the efficient

performance of the finishing process in removing unwanted residual layers resulting from the machining process. The operating variables exhibited varying effects, with the feed rate being the most influential factor, followed by the tool rotational speed, and finally, the abrasive particle size, which was considered the least influential factor. In Figure 17, improvement in surface roughness (SR) after magnetic abrasive finishing (MAF) process as compared to the initial values obtained by EDM. The obtained results indicate a definite improvement, since SR decreased significantly after MAF for different operating conditions, which demonstrates the efficiency of the finishing technique to create smoother surfaces.

Microstructural effects of spark-generated heat, SEM images obtained after EDM (Figure 10) reveal typical thermally-induced features: re-solidified globules, micro-craters and fine surface cracks, all consistent with the formation of a recast (white) layer and a heat-affected zone (HAZ) caused by the rapid melt–vaporize–quench cycle. Increasing current and pulse-on time intensified these features, in line with the observed rise in SR. After MAF, SEM observations (Figure 15) show a marked reduction of re-solidified debris and burrs, smoother crater rims, and improved surface uniformity, indicating partial removal/leveling of the recast layer and mitigation of thermally-induced defects. These qualitative microstructural changes support the quantitative decrease in SR reported in Table 12.

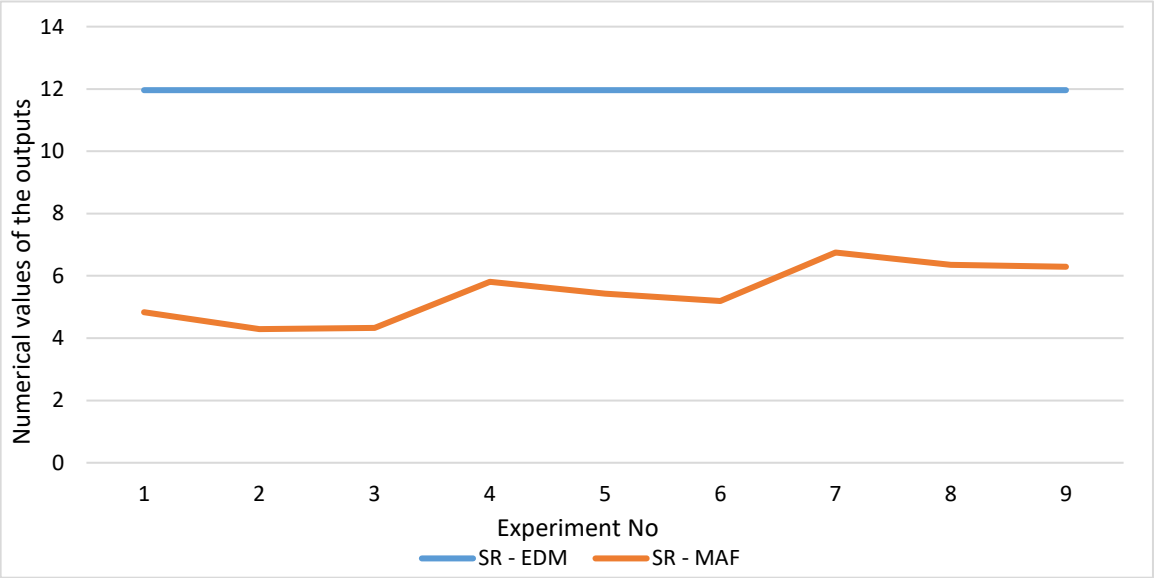

Figure 17: The reduction in surface roughness after applying

5. Conclusion

This study integrates EDM machining of complex models with MAF finishing and uses non-contact laser scanning to quantify surface roughness where contact methods are limited.

1) From the EDM experiments on complex samples, current was the most influential factor: metal removal and surface roughness both increased with increasing current due to higher spark energy. Pulse duration had a moderate effect in the same direction, while the working gap had little effect.
2) A multi-objective analysis (higher MRR, lower SR) identified the optimal EDM setting as Ip = 24 A, Ton = 200 µs, Gap = 8 mm for both designs. Best single responses were: MRR = 25.1024 mm³/min at Ip = 42 A, Ton = 300 µs, Gap = 8 mm, and SR = 11.6674 µm at Ip = 24 A, Ton = 150 µs, Gap = 5 mm.
3) The MAF finishing process was highly effective on the EDM-machined complex surfaces: SR decreased from 11.9169 µm to ≈4.29 µm (64.02%), demonstrating efficient removal of residual layers generated during machining.
4) At this stage of the finishing process, the statistical analysis revealed that the feed rate was the most influential factor, followed by the spindle speed, with the particle size having the least effect. SEM observations corroborated that MAF mitigates thermally-induced EDM defects by leveling the recast layer and removing re-solidified debris, which explains the substantial reduction in SR.
5) The laser scanning technology has proven its effectiveness in obtaining the best and most accurate results when examining complex, uneven surfaces.

Author contributions

Conceptualization, **S. Taqi; W. Hamdan** and **S. Shather**; data curation, **S. Taqi**; formal analysis, **S. Taqi**; investigation, **S. Taqi**; methodology, **S. Taqi**; project administration, **S. Shather**; resources, **S. Shather** and **W. Hamdan**; software, **S. Taqi**; supervision, **S. Shather** and **W. Hamdan**; validation, **S. Taqi, S. Shather,** and **W. Hamdan**; visualization, **S. Taqi**; writing—original draft preparation, **S. Taqi**; writing—review and editing, **S. Shather** and **W. Hamdan**. All authors have read and agreed to the published version of the manuscript.

Funding

This research received no specific grant from any funding agency in the public, commercial, or not-for-profit sectors.

Data availability statement

The data that support the findings of this study are available on request from the corresponding author.

Conflicts of interest

The authors declare that there is no conflict of interest.

References

[1] V. Singh, S. K. Pradhan, Optimization of EDM process parameters: a review, Int. J. Emerg. Technol. Adv. Eng., 3 (2014) 1–11.

[2] A. Y. Jiao, H. J. Quan, Z. Z. Li, Y. H. Zou, Study on improving the trajectory to elevate the surface quality of plane magnetic abrasive finishing, Int. J. Adv. Manuf. Technol., 80 (2015) 1613–1623. https://doi.org/10.1007/s00170-015-7136-9

[3] A. P. Tiwary, B. B. Pradhan, B. Bhattacharyya, Study on the influence of micro-EDM process parameters during machining of Ti–6Al–4V superalloy, Int. J. Adv. Manuf. Technol., 76 (2015): 151–160. https://doi.org/10.1007/s00170-013-5557-x

[4] J. Zhang, L. Wang, L. Jing, Static Analysis of Manipulator Based on SolidWorks and ANSYS Workbench, J. Phys.: Conf. Ser., 2477, 2023, 012034. https://doi.org/10.1088/1742-6596/2477/1/012034

[5] Onwubolu, G .C. Introduction to SolidWorks: A Comprehensive Guide with Applications in 3D Printing; 1st ed. USA: CRC Press, Inc.; 2016.

[6] B. Jabbaripour, M. H. Sadeghi, S. Faridvand, M. R. Shabgard, Investigating The Effects Of EDM Parameters On Surface Integrity, MRR And TWR In Machining of Ti–6al–4v, Mach. Sci. Technol., 16 (2012) 419–444. https://doi.org/10.1080/10910344.2012.698971

[7] M. A. C. Abdullah, A. Yahya, W. Shukri, Integrated Control of Electrical Discharge Machining (EDM) using PSoC, J. Phys.: Conf. Ser., 1529 , 2020, 042087. https://dx.doi.org/10.1088/1742-6596/1529/4/042087

[8] El-Hofy H. Advanced Machining Processes Nontraditional and Hybrid Machining Processes; 1st ed. McGraw Hill; 2005.

[9] Xie H, Zou Y., Investigation on Finishing Characteristics of Magnetic Abrasive Finishing Process Using an Alternating Magnetic Field, Machines, 8 (2020) 75. https://doi.org/10.3390/machines8040075

[10] K. Anjaneyulu, G. Venkatesh, Review on Experimental Investigation of Magnetic Abrasive Finishing process, IOP Conf. Ser.: Mater. Sci. Eng., 1145, 2021, 012066. https://doi.org/10.1088/1757-899X/1145/1/012066

[11] B. Girma, S. S. Joshi, M. Raghuram, R. Balasubramaniam, An experimental analysis of magnetic abrasives finishing of plane surfaces, Mach. Sci. Technol., 10 (2006) 323-340. https://doi.org/10.1080/10910340600902140

[12] M. Alotaibi, B. Honarvar Shakibaei Asli, M. Khan, Non-Invasive Inspections: A Review on Methods and Tools, Sensors, 21 (2021) 8474. https://doi.org/10.3390/s21248474

[13] F. Rodríguez, I. Cotto, S. Dasilva, P. Rey, K. Van der Straeten, Speckle characterization of surface roughness obtained by laser texturing, Procedia Manuf., 13 (2017) 519–525. https://doi.org/10.1016/j.promfg.2017.09.077

[14] S. S. Kumar, M. Uthayakumar, S. T. Kumaran, P. Parameswaran, E. Mohandas, Electrical discharge machining of Al (6351) alloy: role of electrode shape, Int. J. Mater. Prod. Technol., 53 (2016) 86–97. https://doi.org/10.1504/IJMPT.2016.076378

[15] T. W. Huang, D. Y. Sheu, High aspect ratio of micro hole drilling by Micro-EDM with different cross-section shape micro tools for flushing process, Procedia CIRP, 95 (2020) 550–553. https://doi.org/10.1016/j.procir.2020.01.161

[16] Y. Q. Laibi, S. K. Shather, Effect of SiC-Cu electrode on material removal rate, tool wear and surface roughness in EDM process, Eng. Technol. J., 38 (2020) 1406-1413. https://doi.org/10.30684/etj.v38i9A.552

[17] A. A. Abdu, I. A. Gul, A. Ruwaida, Review on Additively Manufactured Electrodes for use in Electro-Discharge Process, J. Electr. Syst., 20-10s (2024) 6919-6930.

[18] M .S. Uddin, V. Santos, R. Marian, Interplay of Process Variables in Magnetic Abrasive Finishing of AISI 1018 Steel Using SiC and Al_2O_3 Abrasives, J. Manuf. Mater. Process., 3 (2019) 29. https://doi.org/10.3390/jmmp3020029

[19] Ahmad S, Singari RM, and Mishra RS., Development of Al_2O_3-SiO_2 based magnetic abrasive by sintering method and its performance on Ti-6Al-4V during magnetic abrasive finishing, Transactions of the IMF, 99 (2021) 94-101. https://doi.org/10.1080/00202967.2021.1865644

[20] Y. Zou, R. Satou, O. Yamazaki, H. Xie, Development of a New Finishing Process Combining a Fixed Abrasive Polishing with Magnetic Abrasive Finishing Process, Machines , 9 (2021) 81. https://doi.org/10.3390/machines9040081

[21] R. Kumar, V. R. Komma, Development of Experimental Setup and Parametric Study of Magnetic Abrasive Finishing Process of Plane Workpieces, NanoWorld J., 9 (2023) S220 – S224 4. https://doi.org/10.17756/nwj.2023-s1-044

[22] M. Shao, D. Xu, S. Li, X. Zuo, C. Chen, G. Peng, J. Zhang, X. Wang, Q. Yang, A review of surface roughness measurements based on laser speckle method, J. Iron Steel Res. Int., 30 (2023) 1897–1915. https://doi.org/10.1007/s42243-023-00930-8

[23] T. G. Raut, M. Y. Shinde, A Review on Optimization of Machining Parameters in EDM, int. J. Innov. Res. Sci. Eng. Technol., 4 (2015) 893-896. http://dx.doi.org/10.15680/IJIRSET.2015.0403013

[24] D. B. Attar, U. S. Pawar, An Overview of Electro Discharge Machining:-A Review, Int. Res. J. Eng. Technol., 4 (2017) 131– 137.

[25] Q. Liu, Q. Zhang, G. Zhu, K. Wang, J. Zhang, C. Dong, Effect of Electrode Size on the Performances of Micro-EDM, Manuf. Process., 31 (2016) 391-396. https://doi.org/10.1080/10426914.2015.1059448

[26] L. Nagdeve, K. Dhakar, H. Kumar, Development of novel finishing tool into Magnetic Abrasive Finishing process of Aluminum 6061, Mater. Manuf. Process., 35 (2020) 1129-1134. https://doi.org/10.1080/10426914.2020.1767295

[27] M. K. Sah, A. Vijaya, H. Singh, Experimental study of the surface finishing of CNC magnetic abrasive finishing based on ANN, Can. Metall. Q., 64 (2025) 1351-1363. https://doi.org/10.1080/00084433.2024.2415726

[28] R. Kumar, V. R. Komma, Recent advancements in magnetic abrasive finishing: a critical review, Eng. Res. Express, 6 (2024) 012504. https://dx.doi.org/10.1088/2631-8695/ad2ef7

[29] M. K. Pradhan, C. K. Biswas, Effect of process parameters on surface roughness in EDM of tool steel by response surface methodology, Int. J. Precis. Technol., 2 (2011) 64-80. https://doi.org/10.1504/IJPTECH.2011.03811

[30] S. B. Chikalthankar, V. M. Nandedkar, S.V. Borde, Experimental investigations of EDM parameters, Int. J. Eng. Res. Dev., 7 (2013) 31-34.

[31] V. T. Tran, M. H. Le, M. T. Vo, Q. T. Le, V. H. Hoang, Optimization design for die-sinking EDM process parameters employing effective intelligent method, Cogent Eng., 10 (2023) 2264060. https://doi.org/10.1080/23311916.2023.2264060

[32] H. Yi, J. Liu, P. Ao, E. Lu, H. Zhang, Visual method for measuring the roughness of a grinding piece based on color indices, Opt. Express., 24 (2016) 17215-17233. https://doi.org/10.1364/OE.24.017215